Journal of Materials Chemistry A

ROYAL SOCIETY OF CHEMISTRY

REVIEW

View Article Online
View Journal | View Issue

Cite this: J. Mater. Chem. A, 2023, 11, 2503

State of the art in the photochemical degradation of (micro)plastics: from fundamental principles to catalysts and applications

Wenxi Li, † Wenxuan Zhao, † Haoyu Zhu, Zhi-Jun Li * and Wanglei Wang*

Plastic, due to its low cost, light weight, and tunable mechanical strength, is one of the most commonly used materials in daily life. However, the massive production of plastics in the last century has resulted in an environmental crisis globally, clogging oceans and poisoning communities around the world. Furthermore, the traditional methods for handling plastic waste, such as incineration and landfill disposal, can easily result in the generation of excessive amounts of microplastics (MPs), which lead to severe environmental pollution and pose a great threat to living organisms. Photocatalytic conversion of plastics to light-weight hydrocarbons and recycling are considered to be promising strategies towards the mitigation of MPs and have attracted a great deal of attention in the last few decades. In this review, a few representative and frontier studies on photocatalysis are presented as green promising methods towards the degradation of (micro)plastics. Initially, we introduce the harmful nature of waste (micro) plastics and discuss the background of photocatalysis. Then, the mechanisms for the photocatalytic degradation of (micro)plastics are presented, followed by the classification of photocatalysts. Also, we highlight conventional inorganic semiconductor oxides (TiO_2, ZnO, *etc.*) and organic–inorganic hybrid composites, including doped and surface-modified nanoparticles. To further improve the efficiency of photocatalytic degradation, several approaches related to reactants, photocatalysts, and reaction conditions are proposed. Finally, based on current photocatalyst-mediated (micro)plastic degradation techniques, we provide some existing limitations and a perspective towards future research directions. This review systematically summarizes the efforts devoted to the photocatalysis of plastic and progress made in the degradation rate.

Received 7th December 2022
Accepted 6th January 2023

DOI: 10.1039/d2ta09523h

rsc.li/materials-a

1. Introduction

Plastics are the third-largest produced materials globally,[1] with their global manufacturing and systematic use since the 1950s. To date, the utilization of plastic products is still popular and would still be on the rise in future owing to their excellent performances such as flexibility and stability,[2] together with low production and user cost. By the end of 2015, the annual plastic production worldwide reached 322 million tons, with its cumulative production reaching 8.3 billion tons.[3] In the absence of an international plastic ban convention or regulation, the universal collective plastic production is expected to grow to 26 billion tons by 2050.[4] Among the great amount of plastics, almost 76% becomes waste plastics. Without proper post-treatment, these plastics can directly lead to serious marine, atmospheric and soil pollution. According to the assessment of the United Nations Environment Programme (UNEP),[5] there is an estimated 75 million to 199 million tons of plastic in the ocean, which is 85% of the total weight of marine debris. Thus, without effective interventions, the amount of plastic waste entering aquatic ecosystems annually is expected to nearly triple to more than 30 million tons per year by 2040.[6]

Nowadays, the most common ways of handling plastics are landfill disposal, incineration and mechanical reprocessing (Fig. 1). Till 2015, the world has produced 6.3 billion tons of waste plastics in total, of which 12% was incinerated and 79% was landfilled or abandoned in the natural environment.[7] It is also estimated that if this status is maintained, 12 billion tons of waste plastic will be buried, incinerated, or discarded into the natural environment.[8] However, these methods are only transient, which cannot alleviate the environmental problems caused by plastics permanently. Furthermore, the abuse of these strategies can lead to severe environmental issues. Among them, plastic landfills need large area of lands and can cause chronic pollution with nearly zero payback;[9] the incineration of plastics causes poisonous gas emissions and deleterious chemical compositions such as CO, furans, dioxins and volatile organic compounds;[10] and even worse, mechanical

State Key Laboratory of Solidification Processing, Atomic Control & Catalysis Engineering Laboratory (ACCEL) School of Materials Science and Engineering, Northwestern Polytechnical University, Xi'an, Shaanxi 710072, P.R. China. E-mail: zhijunli@nwpu.edu.cn; lwang@nwpu.edu.cn

† These authors contributed equally to this work.

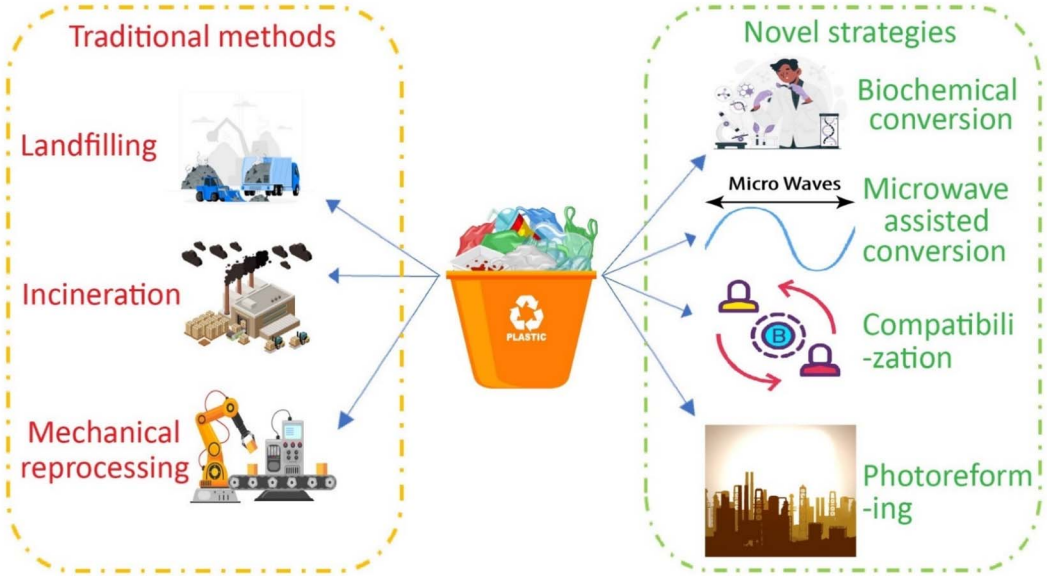

Fig. 1 Traditional and novel ways for the disposal of plastics.

reprocessing requires presorting and damages their mechanical performances.[11] All these physical methods have no significant effects on reducing the amount of castoff plastics and can inversely cause more severe environmental problems with the generation of microplastics. To date, microplastics have been found in seawater, seafloor sediment and even in human blood and lungs, which is much more dangerous than the influence caused by common plastic wastes.[12]

Compared to the typical ways of managing waste plastics, innovative chemical techniques for the degradation of plastics are emerging, which are more environmentally friendly, productive, and can even convert plastics into value-added products (Fig. 1),[13] including biochemical conversion, microwave-assisted conversion, plasma-assisted conversion, supercritical water conversion, compatibilization, pyrolysis, gasification, polymer design and modification, and photoreforming.[14] In addition to their environmentally friendly nature, these approaches are similar, exhibiting advantages and disadvantages. On the one hand, they can decrease the time for plastics to decompose, which takes hundreds of years employing traditional methods, while that for emerging strategies is a few days and even a few hours.[15] Also, during the degradation processes, clean energy and high-value-added products are produced, contributing to the achievements of superior commercial benefits.[16] On the other hand, the shortcomings of these approaches are also prominent due to their low yielding rate and significant cost.[17] Although chemical disposal methods can avoid the production of detrimental substances to a large extent, they lack product regulation and have an extremely low energy efficiency.[18,19] Besides, presorting is required in most strategies, further raising the cost of investments.[15] Also, although quality corrosion and recovery loss are largely avoided compared with conventional methods,[20] these drawbacks greatly hinder their promotion. To achieve the large-scale decomposition of plastic wastes, improving the chemical recycling and upcycling of (micro)plastics are necessary and researchers have been devoted to eliminating the above-mentioned limitations. Among the novel chemical methods for the degradation of plastics, photocatalysis is a superior method to overcome these defects. Thus far, many studies have elaborated the many strengths of photocatalysis in decomposing (micro)plastics as a rapid and stable technique with a relatively high efficiency.[21]

In contrast to other thermochemical and biochemical routes, which may require high energy consumption and harsh reaction conditions such as extremely high temperature and pressure, photocatalysis is comparatively greener and cheaper owning to its suitable energy input and moderate reaction conditions applying sunlight or UV light as the energy source under ambient temperature and pressure.[22] Photocatalysis has a promising outlook in environmental protection due to its redox property,[23] which is related to the excitation of valence electrons to the conduction band and the valence band holes can work as oxidizing agents.[24] Generally, photocatalysis is carried out in cooperation with several steps of hydrogen evolution reaction and oxygen evolution reaction,[25] finally generating H_2O, CO_2 and other value-added chemical products such as H_2 and low-molecular weight organic matter.[13] TiO_2 is the earliest photocatalyst, which was first reported in 1974,[26] with a comprehensive review on the degradation of polyolefins and extensive research on photocatalysis in the field of inorganic semiconductor materials carried out consecutively in the next few decades. Subsequently, numerous studies were conducted on different types of photocatalysts such as organic materials and hybrid materials. Many reviews have focused on photocatalysis and concluded that this burgeoning way of disposing plastics is appropriate from several perspectives.[13,27–30] Chen *et al.* concentrated on the different

reaction paths, advanced representative catalyst systems and converted products in their work.[31] Castilla-Caballero and coworkers introduced various photocatalysts in a chronological order and further evaluated the degree of plastic degradation using techniques such as weight loss, molecular weight determination and carbonyl index.[32] Chu *et al.* emphasized the transformation from plastics to materials, chemicals and access fuels through selective C–C and C–H bonds.[22] Du *et al.* classified solid wastes and elaborated the strengths of cooperatively coupling hydrogen production with the photodegradation of solid wastes.[30] Karimi *et al.* demonstrated the post-synthetic modifications of plastic wastes to improve the degradation effect and acquire the desired products.[33] Zheng and coworkers divided state-of-the-art techniques into two categories, and summarized several catalysis methods with their present situations and potential applications.[34] Zhang *et al.* reviewed solar-driven catalytic plastic upcycling under mild conditions. They also discussed how to precisely and selectively produce high value-added chemical products.[35] However, little attention has been given to the classification of photocatalysis based on the constituents and the recent advancements in achieving the intended effect of photocatalytic degradation of plastics and enhancing the feasibility of its widespread application.

In this review, we focus on studies on different types of photocatalysts and various means of optimizing the photocatalysis performance. This review aims to provide an organized and systematic overview of the progress achieved in the photocatalysis of (micro)plastics, exploring aspects that may affect the processes and outcomes of photocatalysis and considering the current limitations and future perspectives in photocatalysis. It is believed that photocatalysis technologies for the degradation of (micro)plastics can achieve significant commercial and environmentally friendly potential in the future.

2. (Micro)plastic feedstocks and fundamental principles of photodegradation

2.1. Plastics

Plastic is a general term for a class of long-chain polymeric materials that can be shaped or molded at a particular temperature and pressure.[36] Due to the properties of plastic such as plasticity, transparency, low density, toughness and low electrical conductivity, it is widely applied in a variety of conditions such as lightweight disposable bags, beverage bottles, food containers and personal protective equipment such as single-use masks, gowns, and gloves.[32] The common plastics encountered are mainly made of high-density polyethylene (HDPE), low-density polyethylene (LDPE), polyvinyl chloride (PVC), polypropylene (PP), and polystyrene (PS) (Table 1).[37] The most well-known classification of plastics is based on their respective engineering behaviours, which are thermoplastic resin and thermosetting resin.[38] In the case of thermoplastic resin, the polymer can be softened by heating, and then remoulded or reshaped repeatedly. Alternatively, thermosetting resin is insoluble, non-melting and cannot be reprocessed by heating. Besides the ordinary categorization, plastics can also be separated into two types based on their chemical

Table 1 The properties and mechanical parameters of some typical plastics

Polymer type	Degree of crystallinity	Tensile strength (MPa)	Elongation at break (%)	Flexural modulus (GPa)	Typical products and applications	Ref.
HDPE	High	20–30	10–1000	1–1.5	Milk bottles, wire and cable insulation, and toys	41
LDPE	Moderate	8–30	100–650	0.25–0.35	Packaging files, grocery bags, and agricultural mulch	42
PVC	Nil	40–50	2–80	2.1–3.4	Pipes, conduits, and home siding, window frames	43
PP	High	30–40	100 = 600	1.2–1.7	Bottles, food containers, and toys	44
PS	Nil	35–50	1–2	2.6–3.4	Eating utensils, and foam food containers	45

Table 2 Some parameters of biodegradable plastics compared with LDPE

Plastics	Melting point (°C)	Tensile strength (MPa)	Elongation at break (%)	Degradation rate	O_2 barrier property	H_2O barrier property	Ref.
LDPE	110	12	148	Nil	Low	High	42
PLA	180	60	6	Moderate	Moderate	Moderate	49
PBS	120	40	400	Fast	—	—	50
PBAT	120	18	750	Moderate	Low	Low	51
PPC	—	13	650	Moderate	High	High	52
PCL	60	20	300	Low	—	Moderate	53
PHA	145	30	10	High	High	High	54
PGA	225	80	10	High	High	High	55

composition.[39] One includes the most frequently used commodity plastics, as listed all above, which consist of polymers with only aliphatic (linear) carbon atoms in their backbone chains. The other type is plastic composed of heterochain polymers whose backbone chains contain carbons, oxygen, nitrogen, and sulphur.[39] Engineering plastics are mostly from this category, for instance, polyethylene glycol terephthalate (PET), polyacetal, polyamide (commonly known as nylon), polytetrafluoroethylene, epoxy, polycarbonate and polyphenylene sulfide.[40]

Currently, under the promotion of plastic restriction, heterochain polymers, which are well-known as biodegradable plastics, have become a type of environmentally friendly material with high demand in the market.[46] Compared with traditional plastics, they are non-toxic, harmless and can be metabolized by microorganisms in the natural environment and degraded swiftly into small molecules such as CO_2, H_2O and methane.[47] According to the composition and preparation method of raw materials, biodegradable plastics can be divided into natural polymer degradable plastics, microbial synthetic degradable plastics, ad chemical synthetic degradable plastics.[48] At present, the biodegradable plastics that are well developed and employed on an industrial scale to a certain degree mainly include polylactic acid (PLA), poly(butylene succinate) (PBS), poly(butylene succinate-co-butylene adipate) (PBSA), poly(-butylene adipate-co-terephthalate) (PBAT), polyhydroxyalkanoate (PHA), polypropylene carbonate (PPA), polyglycolic acid (PGA), and polycaprolactone (PCL).[48] As substitutes for the widely used typical plastic PE, Table 2 shows the evaluation of biodegradable plastics and LDPE from different perspectives.

To some extent, biodegradable plastic can indeed alleviate the white pollution problem that has plagued human beings for a long time,[47] but it still has many problems at present. Firstly, the degradation conditions of biodegradable plastics are harsh given they can only be rapidly degraded under compost conditions.[56] Secondly, most biodegradable plastics are made from food. Taking PLA as an example, it is made from corn starch or the sugar found in sugar cane and sugar beets.[57] Thus, if the situation does not improve, there will be less food available for humans to eat in the future if the production of biodegradable plastics continues to increase, leading to a severe food race between plastics and humans. Thirdly, the prohibitive cost of biodegradable plastics will be a significant factor limiting their use for at least five years.[58]

2.2. Microplastics

Microplastics are defined as plastic particles with a size of less than 5 mm in diameter,[59] which originate from two sources, with the main on being the degradation of numerous plastic products under conventional disposal strategies.[60] The second source of microplastics is their intentional addition to products such as pesticides, diapers, detergents, cosmetics, pharmaceuticals, and paint products.[60] Subsequently, with the abuse of these products, microplastics are forced into the biosphere and food chain, causing hormone disruption, cancer, and developmental and reproductive problems.[61] In studies about microplastics worldwide, waterways, particularly in aquatic animals, rivers and lakes, are one of the most enriched places where microplastics exist. Data suggests that there are 50 particles per serving of commercially cultured oysters, 90 particles per serving of commercially cultured mussels,[62] and 1 particle for every 8 gallons of Great Lakes tributary water.[63] On average, there were 1285 particles per square foot of river sediment[64] and 112 000 particles per square mile of Great Lakes water.[65] Even worse, microplastics have been observed in 12% of freshwater fish.[66] Additionally, 0.54 mg kg^{-1} microplastics was found in agricultural land located at Loess Plateau in China.[67] To date, microplastics have been detected globally, ranging from industrial estates to places that are off the beaten track, such as the polar regions.[68] Considering the huge impacts that microplastics may have on ecosystems, the benefits of employing plastics are unworthy of consideration and the omnipresent contamination caused by microplastics should be a global concern. In 2015, USA set out a Microbead-free Water Act to prohibit the introduction or manufacture of cosmetics containing intentionally added plastic microbeads.[69] In 2016, an international Pollution Management and Environmental Health (PMEH) program was unveiled by the World Bank to help countries reduce air, land and marine pollution and raise the awareness of the environmental circumstances and pollution issues amongst policy makers and relevant stakeholders.[70] In 2019, the European Union also proposed a resolution to handle the microplastic problem in WWTPs, together with limits for the quantity of microplastics in sewage sludge and treated wastewater.[71]

Microplastics are classified depending on the path through which they enter the natural environment and ecosystem.[72] Primary microplastics are products manufactured specifically as mentioned above, which enter the terrestrial ecosystem through atmospheric deposition and their employment in agricultural lands.[73] Secondary microplastics come from larger plastics that break into small pieces with the help of physical, chemical, mechanical and biological activities.[73] Microplastics originating from the improper disposal of plastics are mostly secondary microplastics, which occupy a large proportion in the environmental network.[73] Despite the small size of microplastics, similar to plastics, they still take hundreds or even thousands of years to decompose, leading to a greater biohazard especially to freshwater ecosystems and marine organisms.[74] When microplastics enter the soil system, they cause great harm directly or indirectly by interacting with or absorbing organic or inorganic toxins, and then disperse in the soil, thus affecting the polymer composition, oxygen concentration and pH value.[75] These factors are essential for the survival of microorganisms and plants in soil and further enter the food chain, posing a risk to all creatures. Even worse, during the aging process, different types of chemicals including phthalates, phenols, and acetophenones can be discharged and long-lasting negative effects are consecutively triggered.[75]

2.3. Mechanism of photocatalytic reaction

When plastics are exposed to ultraviolet or sunlight irradiation alone, their polymer macromolecules can directly absorb photons and generate excited states, leading to chain scission,

Table 3 The general photocatalytic reactions of (micro)plastics

Photocatalytic reactions in oxygen-rich atmosphere:	
Photocatalyst + $h\nu \rightarrow h_{(VB)}^{+} + e_{(CB)}^{-}$	1
$O_2 + e_{(CB)}^{-} \rightarrow O_2^{\bullet -}$	2
$H_2O + h_{(VB)}^{+} \rightarrow \cdot OH + H^{+}$	3
$O_2^{\bullet -} + 2H^{+} + e_{(CB)}^{-} \rightarrow H_2O_2$	4
$H_2O_2 + h\nu \rightarrow 2^{\bullet}OH$	5
$H_2O_2 + O_2^{\bullet -} \rightarrow {}^{\bullet}OH + OH^{-} + O_2$	6
$H_2O_2 + e_{(CB)}^{-} \rightarrow {}^{\bullet}OH + OH^{-}$	7
$^{\bullet}OH$ or $O_2^{\bullet -}$ + (micro)plastics → intermediates + products	8
Photocatalytic reactions in inert atmosphere:	
Photocatalyst + $h\nu \rightarrow h_{(VB)}^{+} + e_{(CB)}^{-}$	1
$H_2O + h_{(VB)}^{+} \rightarrow {}^{\bullet}OH + H^{+}$	9
$H^{+} + e_{(CB)}^{-} \rightarrow H_2$	10
$h_{(VB)}^{+}$ or $^{\bullet}OH$ + (micro)plastics → Selective valuable organic products	11

branching cross-linking and oxidation reactions.[76] However, it takes at least hundreds of years for plastics to degrade.[77] Consequently, to achieve the photodegradation of plastics, suitable catalysts play an essential role throughout the process. The mechanism of photocatalysis has been extensively studied, especially under the catalysis of semiconductors. Below we explain the principles of photocatalysis in detail.

When plastics are disposed in the presence of photocatalysts, briefly, their degradation can be attributed to the following procedures: (i) capturing energy from light to produce electron–hole pairs, (ii) aggregating charge from the interior homogeneous dispersal of the photocatalysts to the surface, and (iii) triggering the redox reactions with the actuation of charges at the interface between reactants and photocatalysts.[78–80] When the photocatalyst absorbs light with sufficiently high energy, electrons are excited from the valence band to the conduction band, $e_{(CB)}-$, and subsequently holes are formed on the valence band, $h_{(VB)}+$.[81] One strategy for photocatalytic reaction is conducted in an oxygen-rich atmosphere, which is called the O_2 evolution reaction (OER).[82] During the degradation process, O_2 reacts with free electrons and is reduced to superoxide anion radicals, $O_2^{\bullet -}$, in the valence band. Simultaneously, the holes in the valence band migrate to the surface and react with H_2O to form hydroxyl radicals, $^{\bullet}OH$, or directly with (micro)plastics (eqn (1)–(3)).[83] Then, the superoxide radicals, $O_2^{\bullet -}$, react with the $e_{(CB)}^{-}$ and H^{+} produced from H_2O to form hydrogen peroxide (eqn (4)), which further reacts with photons, superoxide radicals, $O_2^{\bullet -}$, and $e_{(CB)}^{-}$ to form hydroxyl radical $^{\bullet}OH$, OH^{-} and O_2 (eqn (5)–(7)), respectively. Superoxide radicals, $O_2^{\bullet -}$, and hydroxyl radicals, $^{\bullet}OH$, are among the most active photocatalytic oxidants, which can efficiently oxidize organic compounds (eqn (8)).[84,85] OER photodegradation treats (micro)plastics as wastes to be degraded and generates highly oxidizing radical species, subsequently leading to nonselective oxidation reactions.[86,87]

Another type of photocatalytic reaction is carried out in inert atmosphere, usually in N_2 or Ar, which is usually called the H_2 evolution reaction (HER).[88] In this case, (micro)plastic wastes function as misplaced hydrocarbon resources, enabling the production of value-added products and H_2.[22] Different from photodegradation with O_2, the holes generated by photons on photocatalysts drive the transformation of (micro)plastics to produce relatively highly selective value-added chemicals (eqn (11)), while the photoinduced electrons react with protons simultaneously to form H_2 (eqn (10)).[89,90] The overall photocatalytic reaction process of (micro)plastics of these two different strategies is summarized in Table 3, and Fig. 2 illustrates their mechanism briefly.

The photocatalytic effect is greatly related to the bandgap of photocatalysts, which can dominate the beginning and ending

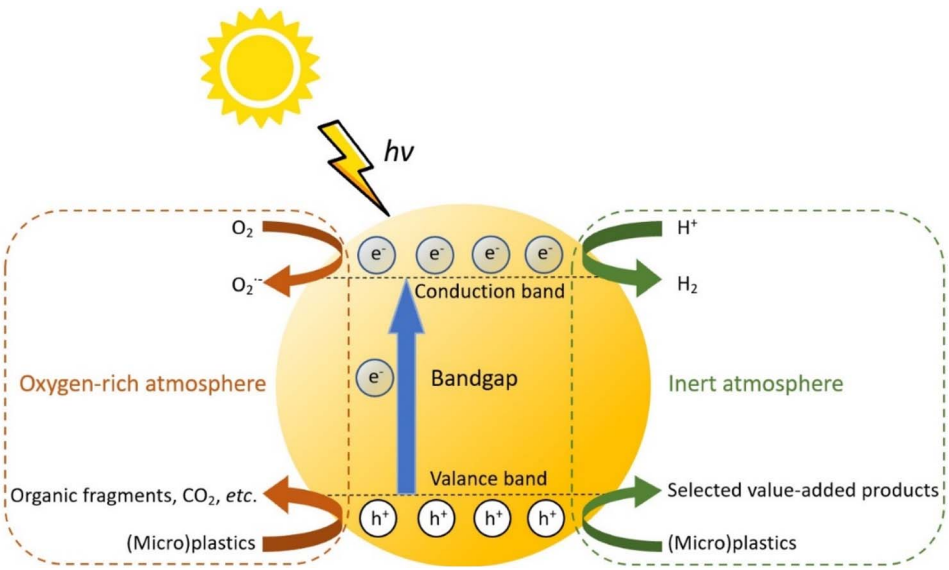

Fig. 2 Schematic diagram of photocatalytic reactions in different environments.

of the reaction process. A narrower bandgap allows (micro) plastic degradation to be conducted in a more facile way, and thus a broader range of materials can be chosen as photocatalysts. For example, TiO_2 and ZnO have bandgaps of 3.2 eV,[91,92] while that of C_3N_4 is 2.7 eV, CN-CNTs-NM is 2.4 eV,[93] polypyrrole (PPy) is 2.2 eV, V-substituted phosphomolybdic acid (VPOM) is 2.19 eV,[94] and PET-derived carbon nitride sheets (PCNS) is 1.82 eV.[95] During degradation, the measured activation energies vary with different properties. In the case of HDPE, the activation energy is in the range of 85.6 ± 27.6 kJ mol^{-1} for the formation of a carbonyl group and 71.5 ± 8.9 kJ mol^{-1} for the formation of vinyl.[96] Meanwhile, in the case of LDPE, the reported activation energy for carbonyl formation fluctuates in the range of 46 kJ mol^{-1} to 95 kJ mol^{-1}. For other degradation products, namely vinyl and hydroxyl groups, the activation energies are lower, which are between 20 kJ mol^{-1} and 46 kJ mol^{-1}.[97–99] The Gibbs energy changes (ΔG^0) have also been reported in some studies. For example, the ΔG^0 for the reforming of lactic acid (a monomer of PLA) is +27 kJ mol^{-1}, while that for ethylene glycol (a monomer of PET) is +9.2 kJ mol^{-1}.[100,101] In general, plastic disposal requires a lower potential, hence lowering the total potential required to accomplish the OER and HER reactions, making photocatalytic degradation more accessible.[22,101] Under this condition, plastic wastes are similar to sacrificial agents, which are easily oxidized by superoxide radicals, hydroxyl radicals or low energy photo-induced holes.[22]

For most doped semiconductors such as Fe/Ag-doped TiO_2, the dopants serve as traps of both $h_{(VB)}^+$ and $e_{(CB)}^-$, aiming to avoid the recombination of electron/hole pairs.[102] Also, semiconductors with other surface modifications can increase the degradation rate because the composite extends the light absorption to the visible spectral region. In these case of hybrid catalysts such as CuPc–TiO_2 and FePc–TiO_2, the dye sensitization is firstly excited to generate $e_{(CB)}^-$ and $h_{(VB)}^+$, and then the electron is shifted to the conduction band of TiO_2 and lead to next series of oxidation–reduction reactions. Additionally, these composites can effectively prevent the aggregation of semiconductors on polymers due to their particular microstructure.[103] Benefiting from these features, composite photocatalysts can achieve a uniform dispersion, higher stability and relatively higher degradation rate compared to other catalysts.

Table 4 Photocatalytic degradation of different plastics and photocatalysts

					Degradation efficiency[a] [%]		
Cat. type	Photocatalyst	Plastic	Light source	Time	Weight loss	Other	Ref.
Inorganic	TiO_2	PVC	Simulated sunlight	300 h	27		104
	Fe/Ag mix doped TiO_2	PE	UV light	300 h	14.34		105
	Ag doped TiO_2	PE	Artificial light	300 h	14.28		105
	BiOI/TiO_2	PVC	UV light	336 h	30.8		106
	TiO_2-MWCNTs	PE	UV light	180 h	35		107
	OMS-2	PE	UV light	288 h	16.5		108
	ZnO	PS	UV light	2 h	16		109
	B–goethite	PE	UV light	300 h	12.6		110
	$FeCl_3$	PS	Blue LED	48 h		78[b]	111
	$FeCl_3$	PS	White light	20 h		23[c]	112
	$Fe_2(SO_4)_3$	PS	LED	66 h		63[b]	112
	C_3N_4	PS	300 W Xenon lamp (150 °C)	24 h		60 ± 4[d]	113
	CdS/CdO_x QDs	PLA	Simulated solar light	24 h		38.8 ± 4[e]	114
	CN_x|Ni_2P	PET	Simulated solar light	8 days		24.5 ± 3.3[e]	100
	CN-CNTs-NM	PET	LED (288 K)	4 h		0.62[f]	93
	VPOM/CNNS	PEG	Visible light	3 h		16.55[g]	115
Organic	Fluorenone	PS	Blue LED	48 h		38 ± 3[b]	116
	pTsOH·H_2O	PS	450 nm, 9 W	15 h		50[b]	117
Hybrid	FePc–TiO_2	PS	Sunlight	12 days	35		103
	PPy/TiO_2	PE	Sunlight	240 h	35.4		118
	$FePcCl_{16}$-TiO_2	PVC	UV light	240 h	50		119
	PAM-*g*-TiO_2	LDPE	UV light	520 h	39.85		120
	T@AIH	LDPE	340 nm Xenon lamp (65 °C)	72 h		54.7[h]	78

[a] Different papers present the degradation rate through different indices. Below we list the results with the data provided in the references and the index is remarked respectively. [b] NMR yield of benzoic acid. [c] Total yield of benzoyl products on a monomer basis. [d] Selectivity (%) = (n(carbon in benzoic acid, acetophenone and benzaldehyde)/(n(carbon in benzoic acid, acetophenone and benzaldehyde) + n(CO_x total))) × 100%, CO_x from solvent oxidation is included. [e] Conversion (%) = 100 × N_{lim}/N100%, N_{lim} is the limiting amount of H_2 obtained from 1 mol of substrate. N100% is the ideal amount of H_2 obtainable from 1 mol of substrate (calculated from chemical reactions listed in the main text). [f] AQY (%) = (number of reacted electrons)/(number of incident photons) = (2 × number of evolved hydrogen molecules)/(number of incident photons) × 100%. [g] Upcycling efficiency, defined as the carbon element recovery efficiency after 36 h reaction: the moles of produced formic acid divided by the moles of carbon atoms in the added plastic. [h] Degradation efficiency.

3. Classification and overview of photocatalysts

Numerous studies have been conducted regarding photocatalytic degradation in the last few decades, and thus it is necessary summarize some of the research (Table 4). We introduce several representative photocatalysts and their performances in the following section and their mechanism will be proposed afterwards.

3.1. Inorganic semiconductor photocatalysts

3.1.1. Bare photocatalysts. The use of TiO_2 as a photocatalyst dates back to 1974, when the effect of TiO_2 pigments on phosphorescence from polyolefins such as PP and LDPE was studied.[121] Allen *et al.* reported that anatase TiO_2 had high photosensitivity and high capacity to capture the phosphorescence emitted by the impurities of the polymers, which contributes to the degradation of these polymers. Since then, many studies have been done on the solid-phase photocatalytic degradation of polymer-TiO_2 composites in relation to the chalking phenomenon (the surface of the polymer erodes gradually).

In 2001, Cho *et al.* studied the photocatalytic degradation of PVC films embedded with TiO_2 particles (0–2 wt%) under ambient air or a nitrogen atmosphere using SEM microscopy, FT-IR and UV-vis spectroscopy, and XPS (Fig. 3).[104] In these experiments, the PVC–TiO_2 composite films consisted of 1.5 wt% of TiO_2 and were 25–30 μm thick, which were irradiated under a 200 W mercury lamp. According to the results, the weight of the PVC–TiO_2 film decreased by 27% with irradiation under air, while the PVC film showed only 10% weight loss under identical experimental conditions. Cho *et al.* reported that the M_w of the composite film steadily decreased with irradiation time. During the process of photodegradation, most of the higher M_w fraction disappeared after 13–15 min of elution and the average M_w was reduced to a third after 300 h irradiation. The average M_w of the pure PVC films was reduced by half in 300 h accordingly, indicating that both the direct photolytic and photocatalytic reaction participated in the bond scission in the backbone of the polymer.

The SEM images of the PVC–TiO_2 composite films showed much more and larger holes on their surface under the ambient air atmosphere compared to merely no holes under a nitrogen atmosphere. This result confirmed the necessity of oxygen for the solid-phase photocatalytic reaction. The SEM images also proved that the active oxygen species generated on illuminated TiO_2 diffused away from the surface into the gas-phase. Most of the oxidizing power of TiO_2 is attributed to the reaction of surface hydroxyl groups on TiO_2 with the valence band holes, generating hydroxyl radicals. The main gaseous products, CO_2 and H_2O, were monitored by using an FT-IR gas cell. Also, HCl, the main product of thermal and direct photolytic degradation of PVC, did not appear, showing that photocatalytic degradation of the PVC–TiO_2 film is an environmentally friendly method.

In 2007, Bandyopadhyay *et al.* reported the photodegradation of polystyrene (PS) using ZnO as a photocatalyst.[109] ZnO had the greatest advantage of absorbing a longer fraction

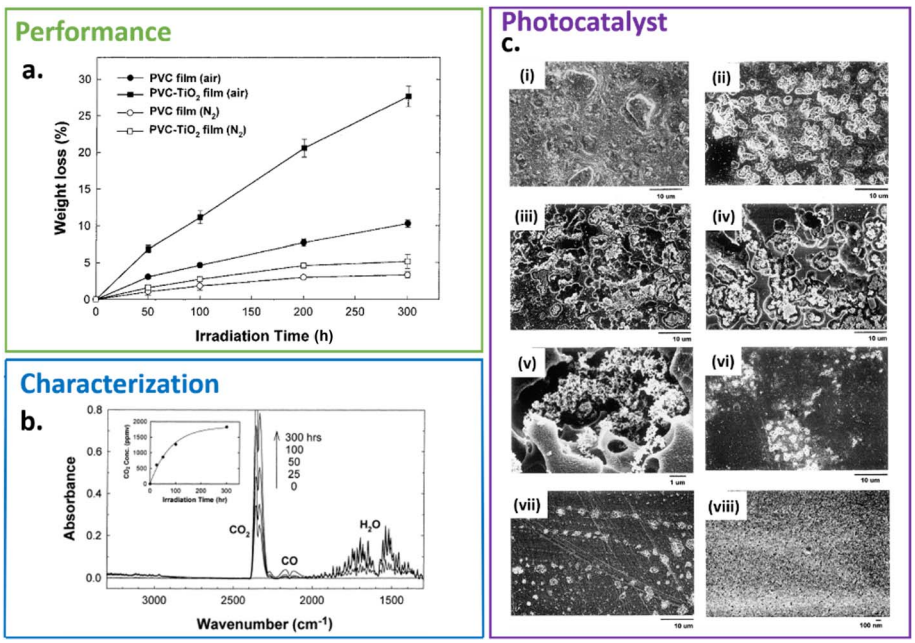

Fig. 3 (a) Weight loss of the pure PVC or PVC–TiO_2 (1.5 wt%) composite films during irradiation under air or nitrogen atmosphere. (b) FT-IR spectra of volatile products evolved from the irradiated PVC–TiO_2 (1.5 wt%) film under air. The inset shows the evolved CO_2 concentration as a function of irradiation time. (c) SEM images of the pure PVC or PVC–TiO_2 (1.5 wt%) composite films. (i) PVC–TiO_2 film before irradiation; (ii) PVC–TiO_2 film, irradiated for 25 h; (iii) PVC–TiO_2 film, irradiated for 50 h; (iv) PVC–TiO_2 film, irradiated for 100 h; (v) PVC–TiO_2 film, irradiated for 100 h (enlarged view); (vi) backside view of the PVC–TiO_2 film, irradiated for 100 h; (vii) PVC–TiO_2 film, irradiated for 100 h under N_2; and (viii) pure PVC film, irradiated for 100 h. Reproduced with permission from ref. 104. Copyright 2001, Elsevier.

of the solar spectrum, and therefore may provide the highest efficiency. The weight loss of the virgin PS as a function of UV exposure time barely increased, while the weight loss upon the addition of 0.1 wt% ZnO to $PS_{0.1}$ increased, showing that ZnO acted as a photocatalyst for the degradation of PS. The weight loss of PS as a function of UV exposure time gradually increased with an increase in ZnO concentration up to 0.5 wt% with respect to PS. The 0.5 wt% ZnO-containing $PS_{0.5}$ showed the highest weight loss. However, when the concentration of ZnO reached 1 wt%, PS hardly showed any weight loss under the experimental conditions. In fact, the rate of photodegradation of PS slowed down significantly when the concentration of ZnO was greater than 0.5 wt%. During the degradation, ZnO, acting as a UV absorber, could transmit the absorbed energy to the C–C and C–H bonds of the PS molecules, which caused cleavage reactions given that this energy was higher than the dissociation energies of these bonds. The dispersion of ZnO in the PS matrix was the most important factor. The better dispersion of ZnO would cause the greater absorption of the polymer macrochains on the metal oxide and higher chances of cleavage reactions by efficient energy transfer to the matrix. AFM was used to investigate the sample surface. The RMS roughness of $PS_{0.5}$ after degradation reached 101 nm, which is about 7-times rougher than $PS_{0.5}$ before degradation, which led by the loss of oxidized materials (mainly as CO_2) from the surface upon UV exposure. The main products of the photodegradation of PS were CO_2 and H_2O, as reflected by the viscosity average molecular weight measurements of the degraded samples.

Liu *et al.* used manganese oxide (OMS-2) as a photocatalyst in the photocatalytic degradation of polyethylene (PE) in 2011.[108] They studied the photocatalytic degradation of PE with OMS-2 in the ambient air under UV and visible light irradiation. During the photodegradation, OMS-2 played a vital role because of its octahedral molecular structure sieves and excellent catalytic properties. OMS-2 powder exhibited remarkable absorbance in the visible region beyond 400 nm. The weight of PE-OMS-2 (0.1 wt%) decreased by 16.5% after 288 h under UV light irradiation, while there was only 4.1% weight loss in the pure PE under the same experimental conditions. In contrast, no weight loss was observed for PE-OMS-2 under visible light irradiation after 128 h, which suggested that visible light irradiation could not induce activity for the photocatalytic degradation of OMS-2. The degradation rate is proportional to the concentration of OMS-2 when it was less than 1.0%. However, a reduction in weight loss was observed with the further addition of OMS-2. The SEM images showed the growth of cavities in the surface of PE-OMS-2 during photodegradation. An increase in the size and depth of the cavities was observed in the PE-OMS-2 films due to the escape of volatile products from the PE matrix, while few changes appeared in the pure PE film. The degradation of PE may start at the PE-OMS-2 interface, where active oxygen species generated on the surface of OMS-2 diffused and etched the polymer matrix, which led the formation of cavities around the OMS-2 particles. The OMS-2 particles irradiated by UV light generated electron/hole pairs in the conduction band and valence band, contributing to the degradation reaction.

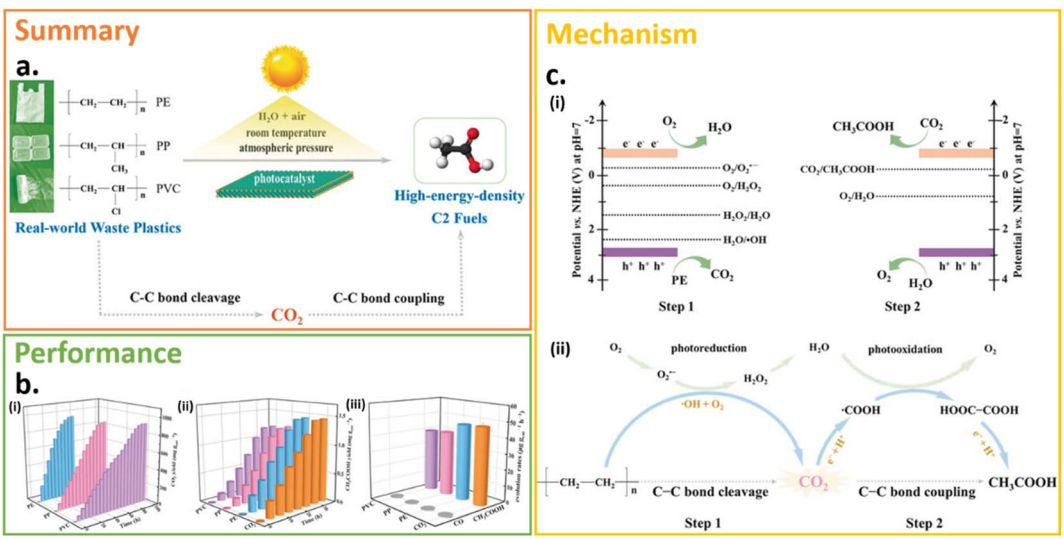

Fig. 4 (a) Schematic illustration of the conversion of various waste plastics into C_2 fuels by a designed two-step pathway under simulated natural environment conditions. Specifically, various plastics were exclusively degraded into CO_2 by photooxidative C–C bond cleavage over a photocatalyst, while the produced CO_2 was further reduced into highly valuable C_2 fuels by photoinduced C–C bond coupling over the same photocatalyst. (b) Photoconversion of various plastics into C_2 fuels under simulated natural environment conditions. (i) Yield of CO_2 during the photoconversion of pure PE, PP, and PVC over the Nb_2O_5 atomic layers, in which the molar ratio of carbon in each plastic and Nb_2O_5 atomic layers is *ca.* 50 : 1. (ii) Yield of CH_3COOH and (iii) evolution rates of CH_3COOH and CO during the photoconversion of pure PE, PP, and PVC, as well as during the photoreduction of pure CO_2 in water. In all the photoconversion tests, each plastic and pure CO_2 have the same number of moles of carbon. (c) Schematic representation of (i) band-edge positions of Nb_2O_5 atomic layers along with the potentials of CO_2, H_2O, H_2O_2, and O_2 redox couples at pH 7 and (ii) proposed two-step C–C bond cleavage and coupling mechanism from pure PE into CH_3COOH under simulated natural environment conditions. Reproduced with permission from ref. 122. Copyright 2020, John Wiley and Sons.

Besides conventional semiconductors such as TiO_2, ZnO and MnO, Jiao *et al.* achieved a 100% photodegradation rate of PE, PP and PVC into CO_2 with single-unit-cell thick Ni_2O_5 layers, at room temperature and ambient pressure within 40, 60 and 90 h in 2020 (Fig. 4).[122] Then, CO_2 was further photoreduced to CH_3COOH, helping to relieve the environmental pollution caused by (micro)plastics and generate value-added multi-carbon fuels simultaneously. Ni_2O_5 is a type of highly stable and earth-abundant semiconductor, and the fabricated single-unit-cell thick Ni_2O_5 can largely maximize the conducting surface, and consequently optimize the photodegradation conversion. Also, commercial PE-, PP- and PVC-based plastic commodities such as food wrap films, single-use bags and disposable food containers could also be photodegraded into CH_3COOH with a smaller yield compared with pure PE, PP and PVC, indicating its possible real-world application.

In 2022, the degradation of PS with $FeCl_3$ was reported by Oh *et al.*, which could promote the upcycling of PS to benzoyl products and primarily benzoic (Fig. 5).[123] Under visible light irradiation, $FeCl_3$ can generate chlorine radicals and abstract C–H bonds from the PS backbone, finally resulting in the cleavage of the C–C bond. In experiments, commercial PS was degraded. After photooxidative degradation, PS with M_w more than 90 kg mol^{-1} was degraded into oligomers (M_n = 0.8 kg mol^{-1}), with up to 23 mol% generation of small-molecule benzoyl products under saturation system of O_2, that is, benzoic acid, benzaldehyde, benzoyl chloride and acetophenone. Compared with benzophenone, which was used in previous research on the degradation of PS degradation, the introduction of chlorine radical in this study enhanced the formation of benzoyl products. Also, $FeCl_3 \cdot 6H_2O$, LiCl, NaCl and NH_4Cl were used as alternatives under identical conditions; however, no improvement in benzoyl product formation was observed.

Later, in the same year, another method was proposed using heterogeneous graphitic carbon nitride (g-C_3N_4) as catalysts under visible light irradiation to degrade PS to aromatic oxygenates such as benzoic acid, acetophenone and benzaldehyde (Fig. 6).[113] Chain oxidation happened primarily, and then the oxidized PS was cleaved. In the experiments, the exceedingly efficient upcycling of PS with the yield of 60% towards organic products was achieved. High selectivity of 74% for benzoic acid or 51% for benzaldehyde in independent experiments was achieved by adjusting the weight hourly space velocity (WHSV) of PS in a flow reaction system. In the circulatory system, with pretreated PS, at 150 °C with a proper ratio of substrate/catalyst (5 : 2) and reaction time (8 h), about 10 mg g_{catal}^{-1} h^{-1} mass-specific reactivity and over 80% selectivity towards benzoic acid were observed, indicating excellent reaction performance under the g-C_3N_4 photocatalyst.

3.1.2. Composite photocatalysts. Liu and coworkers prepared a novel photodegradable polyethylene–boron–goethite (PE–B–goethite) composite film by embedding boron-doped goethite in the commercial polyethylene.[110] The photocatalytic efficiency of the boron-modified goethite catalyst was

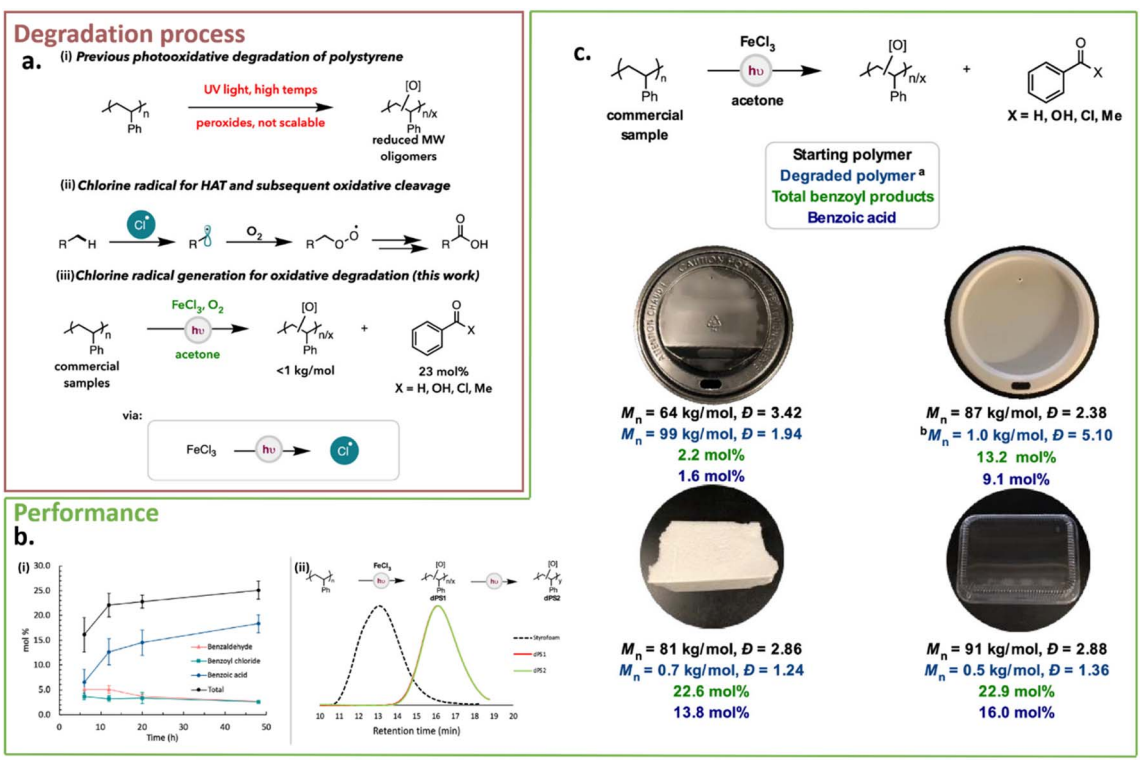

Fig. 5 (a) Proposed upcycling of polystyrene. (b) (i) Scatter plot for benzoic acid, benzaldehyde, and benzoyl chloride at each time point for PS degradation under O_2. (ii) Degradation profile of oxidized PS in the absence of $FeCl_3$. (c) Commercial PS degradation. Reproduced with permission from ref. 123. Copyright 2022, the American Chemical Society.

improved under UV light and visible light irradiation. Compared to goethite, the B–goethite composite powder had a decreased band gap after boron doping, exhibiting a remarkable absorbance in the visible region from 400 to 600 nm. The dispersion also improved given that that boron entered the lattice spaces of goethite and prevented crystal growth. The weight loss of PE–B–goethite (0.4 wt%) was 12.6% under 300 h UV irradiation in the air, while only 2.6% for pure PE and 9.5% for PE–goethite, indicating the higher photocatalytic activity of boron-doped goethite. The weight loss of PE–B–goethite was not detected under visible light irradiation after 128 h, which suggested that visible light irradiation could not induce activity for the photocatalytic degradation of B–goethite.

Yang *et al.* improved the photocatalytic performance of nano-TiO_2 by embedding a nano-TiO_2 photocatalyst modified by bismuth oxyiodide (BiOI), preparing a new type of photodegradable PVC–BiOI/TiO_2 nanocomposite film.[106] Nano-TiO_2 is considered a good photocatalyst because of its high reactivity, good photostability, low cost and non-toxicity, but it can only absorb UV light with a wavelength of less than 387 nm.[124,125] Due to the heterostructure of BiOI/TiO_2, the combination of nano-TiO_2 and BiOI achieved more efficient separation of the electron–hole pairs and higher photocatalytic activity. The absorbance of the PVC–BiOI/TiO_2 nanocomposite film was higher than that of the PVC–TiO_2 nanocomposite film and pure PVC film. After 336 h UV light irradiation, the weight of the pure PVC film decreased by 3.2%. The weight loss of the PVC–TiO_2 nanocomposite film reached 20.8% after 336 h of irradiation, while that of the PVC–BiOI/TiO_2 nanocomposite film was 30.8%, which was 1.5-times higher than that of the PVC–TiO_2 nanocomposite film. This proved that the photocatalytic performance of the nano-TiO_2-containing PVC film was remarkably promoted by the BiOI modifier. They reported that the concentration of BiOI influenced the weight loss rates of the PVC–BiOI/TiO_2 nanocomposite film, and when the mass ratio of BiOI to TiO_2 reached 0.75%, the degradation rate reached its peak, indicating that at this time, the PVC–BiOI/TiO_2 nanocomposite film had the best photocatalytic activity. When the mass ratio exceeded 0.75%, the weight loss rate decreased drastically but was still higher than that of the PVC–TiO_2 nanocomposite film. The decreasing intensities of the C–H groups and the increasing intensities of the carbonyl groups shown in the FT-IR spectra of the PVC–BiOI/TiO_2 nanocomposite film were more pronounced than that of the PVC–TiO_2 nanocomposite film, suggesting that the photooxidation reaction occurred in the composite film. The weight loss rate of the PVC–BiOI/TiO_2 nanocomposite film (TiO_2: 2 wt%) changed

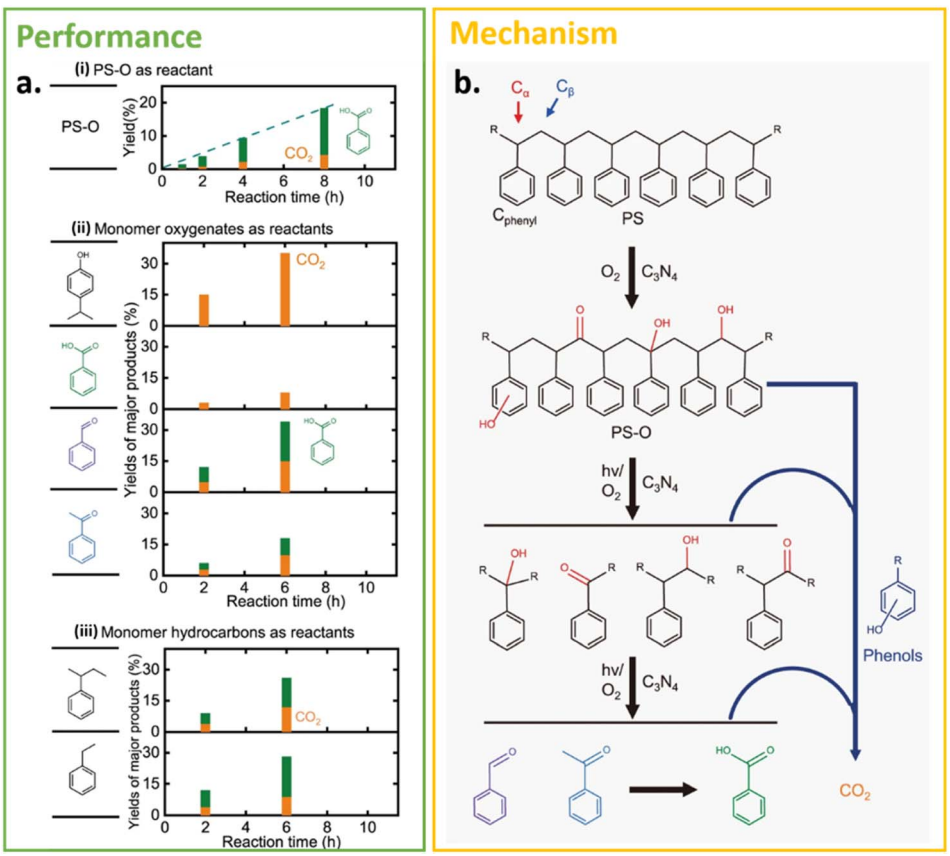

Fig. 6 (a) Catalytic performances of (i) oxygen-treated polystyrene, (ii) oxygenate monomers, and (iii) hydrocarbon monomers as reactants under standard reaction conditions. Reaction conditions: 50 mg g-C_3N_4, 20 mg reactant, 30 mL acetonitrile, 10 bar O_2, irradiated by 300 W Xenon lamp at 150 °C. (b) Proposed reaction pathway of polystyrene photo–oxidation reaction. Reproduced with permission from ref. 113. Copyright 2022, Springer Nature.

at different mass ratios of BiOI to TiO_2 under UV light irradiation.

In 2018, Uekert *et al.* reported the preparation of an economical photocatalyst, *i.e.*, CdS/CdO_x quantum dots, and employed it for the visible light-driven photodegradation of PLA, PET and PUR.[114] After degradation, these waste plastics were converted into H_2 and organic products such as formate, acetate, and pyruvate at ambient temperature and pressure. Under an N_2 atmosphere, PLA, PET and PUR exhibited higher activities and could generate larger quantities of H_2 compared to other types of polymers. After photocatalytic reactions, the activity for the degradation of PLA, PET and PUR was 64.3 ± 14.7, 3.42 ± 0.87, and 0.85 ± 0.28 $mmol_{H_2}\ g_{CdS}^{-1}\ h^{-1}$, respectively. Individually, the overall H_2 production of the three plastics reached 3.09 ± 0.15, 0.21 ± 0.04, and 0.04 ± 0.01 $mmol_{H_2}\ g_{substrate}^{-1}$, respectively. In controlled trials without UV irradiation ($\lambda > 400$ nm), photoreforming still continued effectively, suggesting that the photocatalyst could function with the utilization of visible light ultimately.

However, this cadmium-containing catalyst makes the subsequent treatment of the plastic degradation system difficult owing to its toxicity. Then, one year later, Uekert *et al.* proposed the use of a nontoxic and reasonably priced carbon nitride/nickel phosphide ($CN_x|Ni_2P$) as a photocatalyst to reform PET and PLA under visible light, generating pure H_2 and various organic chemicals (Fig. 7).[100] Different from CdS/CdO_x,

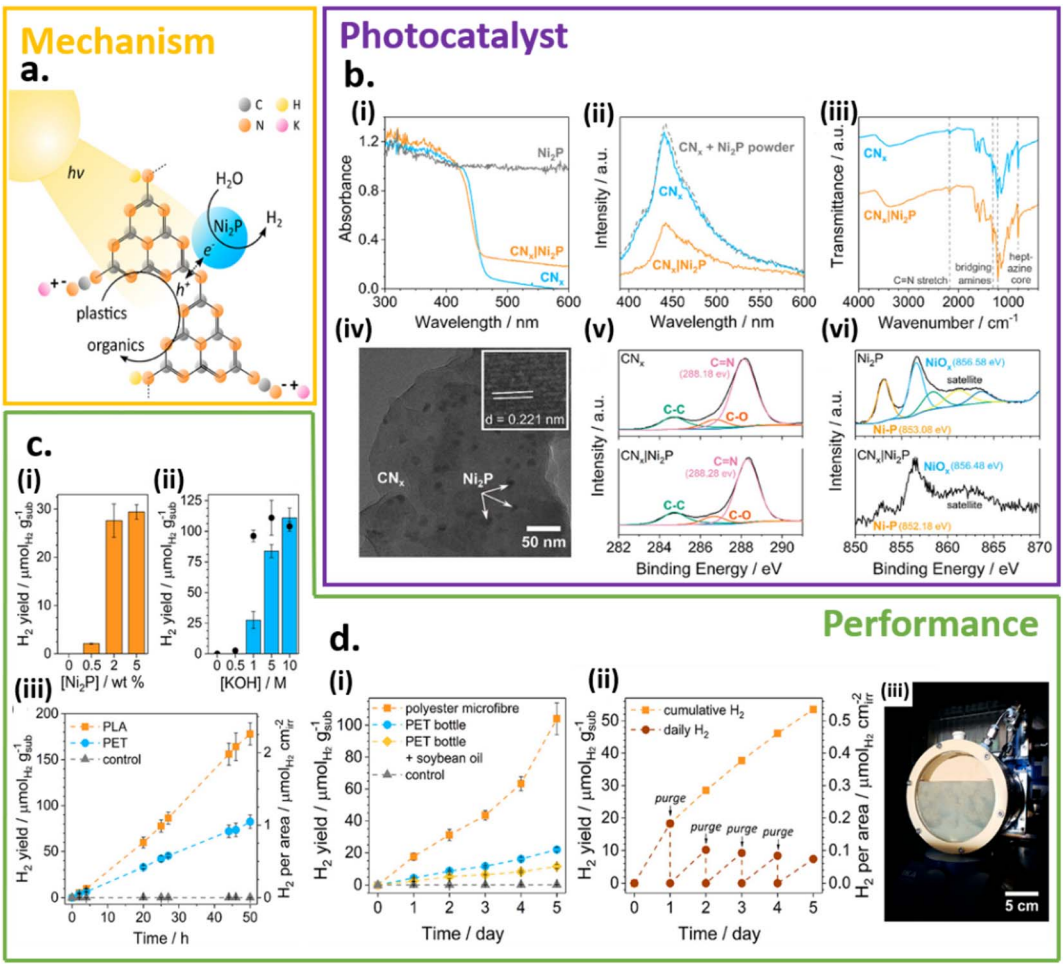

Fig. 7 (a) Schematic diagram of the polymer photoreforming process using $CN_x|Ni_2P$ photocatalyst. (b) Characterization of the $CN_x|Ni_2P$ (2 wt%) photocatalyst. Comparison of (i) diffuse-reflectance UV-vis, (ii) emission ($\lambda_{ex} = 360$ nm, $\lambda_{em} = 450$ nm), and (iii) FTIR spectra of CN_x and $CN_x|Ni_2P$. (iv) TEM image of the $CN_x|Ni_2P$ catalyst, with the inset showing the lattice spacing of Ni_2P. XPS spectra of (v) C_{1s} edge for CN_x and $CN_x|Ni_2P$ and (vi) Ni_{2p} edge for Ni_2P and $CN_x|Ni_2P$. (c) Photoreforming of PET and PLA with $CN_x|Ni_2P$. Optimization of (i) Ni_2P loading and (ii) KOH concentration for the photoreforming of PET (after 20 h irradiation). Black circles in (ii) mark H_2 evolution per gram of substrate over $CN_x|Pt$ (2 wt%) under the same conditions. (iii) Long-term photoreforming of PET and PLA. Conditions unless stated otherwise: $CN_x|Ni_2P$ 2 wt% (1.6 mg mL^{-1}), pretreated PET (25 mg mL^{-1}), aqueous KOH (1 M, 2 mL), and simulated solar light (AM 1.5 G, 100 mW cm^{-2}, 25 °C). (d) Photoreforming of nonrecyclable plastic waste. (i) Long-term photoreforming of polyester microfibers, a PET bottle, and an oil-coated PET bottle. (ii) Upscaled photoreforming of polyester microfibers, where sample was purged every 24 h. Conditions: $CN_x|Ni_2P$ (1.6 mg mL^{-1}), 1 M KOH (2 mL for part (i) and 120 mL for part (ii)), pretreated microfibers (5 mg mL^{-1}) or PET bottle (25 mg mL^{-1}) without or with soybean oil (5 mg mL^{-1}), simulated solar light (AM 1.5 G, 100 mW cm^{-2}). (iii) Photograph of the batch reactor in use. Reproduced with permission from ref. 100. Copyright 2019, the American Chemical Society.

this type of noble-metal- and Cd-free photocatalyst exhibited enhanced stability, catalytic efficiency and charge separation, achieving photostability for at least 5 days. Also, 82.5 ± 7.3 and 178 ± 12 $\mu mol_{H_2}\ g_{sub}^{-1}$ H_2 were produced from PET and PLA after 50 h of irradiation, with the external quantum yields of 0.035% ± 0.005% and 0.101% ± 0.018% for PLA at $\lambda = 430$ nm, respectively. The H_2 conversion reached 4.4% ± 0.6% and 1.6% ± 0.2% after 8 days of photoreforming with PET and PLA, respectively. It was noted that the reaction system was still active after 8 days, indicating that the H_2 conversion may achieve a higher value if the photodegradation process lasted for a longer time. Actually, the photoreforming of ethylene glycol showed 50% H_2 conversions after 18 days. At a higher pH condition, elevated H_2 conversions were observed as 24.5% ± 3.3% for PET and 6.7% ± 0.8% for PLA.

In 2022, Gong *et al.* developed an *in situ*-derived carbon nitride–carbon nanotube–NiMo hybrid *via* NiMo-assisted catalysis route (CN–CNTs–NiMo), which proved to be an efficient and stable photocatalyst (Fig. 8).[93] The NiMo nanoparticles acted as a co-catalyst to improve the photocatalytic activity of PET because of its excellent HER electrocatalytic activity and durability in alkaline condition. CNTs exhibited superior chemical stability, large surface area and excellent electron mobility in alkaline condition.[126,127] The integration of NiMo nanoparticles and CNTs into a heterogenous structure is an effective strategy to promote the transfer of electrons from CN to NiMo. According to their study, the strong π–π interactions between CNTs and CN can promote electron transfer from CN to NiMo, increase the carrier lifetime and improve the photocatalytic activity. The photocatalytic activity of CN–CNTs–NiMo for the photodegradation of PET was around 14 times higher than that of CN. After normalization to exclude the influence of the surface area of the photocatalyst, CN–CNTs–NiMo still showed nearly 2-times higher hydrogen evolution rate with PET than CN.

Also, based on the advantages of carbon nitride, C_3N_4, Xing *et al.* designed and fabricated a self-assembly *Z*-scheme heterostructure of V-substituted phosphomolybdic acid clusters/g-C_3N_4 nanosheets (VPOM/CNNS), which is an efficient and sustainable strategy for the photodegradation of various plastic

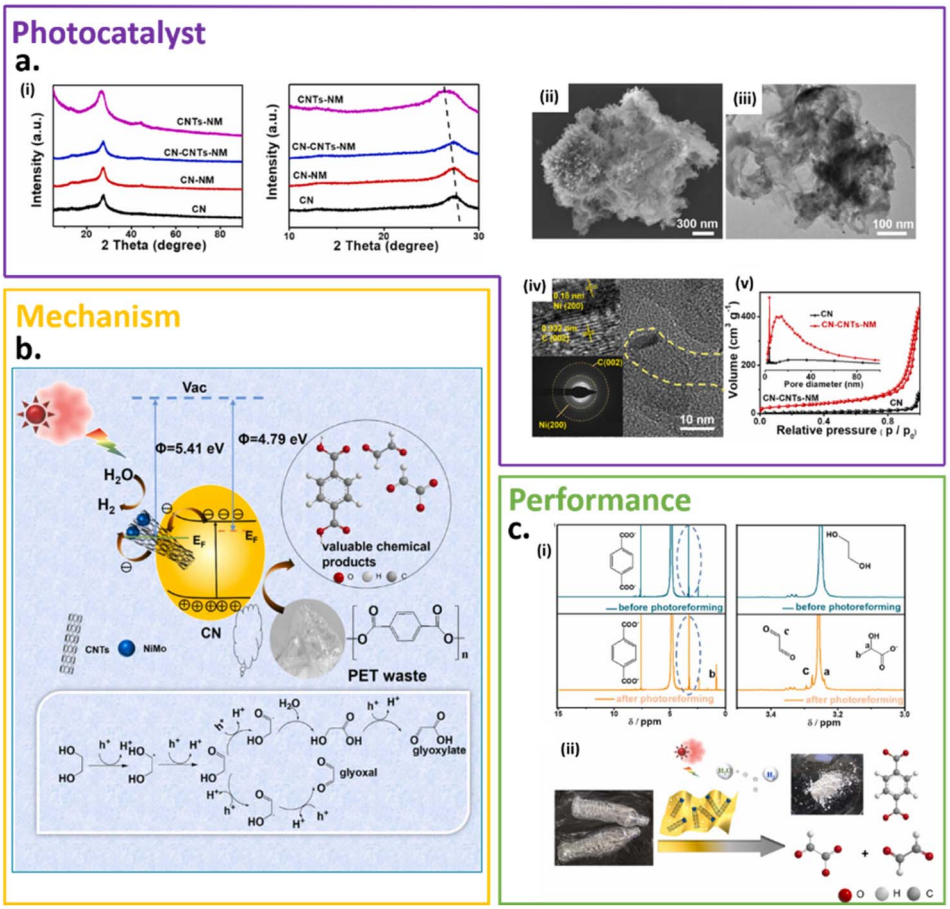

Fig. 8 (a) (i) XRD patterns of CN, CN–NM, CN–CNTs–NM and CNTs–NM. (ii) SEM images of CN–CNTs–NM. (iii) Low-magnification TEM and (iv) HRTEM image and SAED pattern of CN–CNTs–NM. (v) N_2 adsorption desorption isotherms of CN–CNTs–NM and CN. (b) Schematic diagram of the process of photoreforming of PET using CN–CNTs–NM. (c) (i) ^1H NMR spectra of PET before and after photoreforming. (ii) Photoreforming of PET to obtain commodity chemicals and H_2 fuel. Reaction conditions: 10 mL KOH (5 M), pretreated PET (50 mg mL^{-1}), and 10 mg CN–CNTs–NM under simulated solar light for 4 h at 288 K. Light resource: simulated solar light, 95 mW cm^{-2}. Reproduced with permission from ref. 93. Copyright 2022, Elsevier.

waste under visible light irradiation (Fig. 9).[115] The bio-mimic *Z*-scheme heterostructure not only promoted the carrier separation, but also reserved the strong redox ability of electrons and holes to participate in the photodegradation of plastics. The VPOM/CNNS *Z*-scheme heterojunction exhibited abundant surface-active sites and short charge transport by rationally modulating the surface charge. VPOM/CNNS could photodegrade various polymers to produce formic acid (HCOOH), which has a wide range of applications in fuel cells and liquid storage for hydrogen energy. The best formic acid production rate of the VPOM/CNNS composite was up to 24.66 μmol h^{-1} g^{-1}, which was 262-times higher than that of pristine CNNS.

3.2. Organic photocatalysts

In 1997, Wéry *et al.* optimized the photodegradation of poly-*p*-paraphenylene vinylene (PPV) by monitoring the substrate temperature and irradiation time by UV-vis absorption. The photodegradation of the tetrahydrothiophenium precursor of PPV could happen under UV irradiation in air at room temperature.[128] In the study by Li *et al.*, they introduced concepts ranging from small-molecule catalysis to polymer deconstruction, as demonstrated by the photodegradation of PS foam on a gram scale *via* the C–H bond oxidation pathway.[116] Inspired by the bond cleavage chemistry of small hydrocarbon molecules, employing a hydrogen atom transfer (HAT) catalyst could handle the challenge of activation and selective chemistry of stable C–H bonds.[129–132] Li *et al.* used an aromatic ketone as the HAT photocatalyst and the photocatalysis was driven by a blue LED under mild temperature and pressure. PS was degraded to form benzoin acid with ~40% yield and other identified monomeric aromatic products with ~20% yield after about 48 h irradiation due to the cleavage of the C–C bonds in the polymer backbone. No reactivity was observed without the photocatalyst or light under the same condition. Only 5 mol% of fluorenone was required to produce benzoic acid with 31% yield at 48 h, while 20 mol% loading of the photocatalyst produced 38 ± 3% yield, proving the photocatalytic role of fluorenone.

In 2022, Huang *et al.* first described a light-driven, acid-catalyzed protocol for the degradation of polystyrene under mild conditions without the need for photosensitizers (Fig. 10).[133] They found that triflic acid (5 mol%, HOTf) could catalyze the photodegradation of PS under 405 nm violet-blue light irradiation with 1 bar O_2 as the oxidant. The products of the photodegradation of PS were isolable formic acid with 72% yield, benzoic acid with 40% yield and benzophenone with 2% yield. Since there were no desirable products without irradiation, light played a significant role in the degradation. This

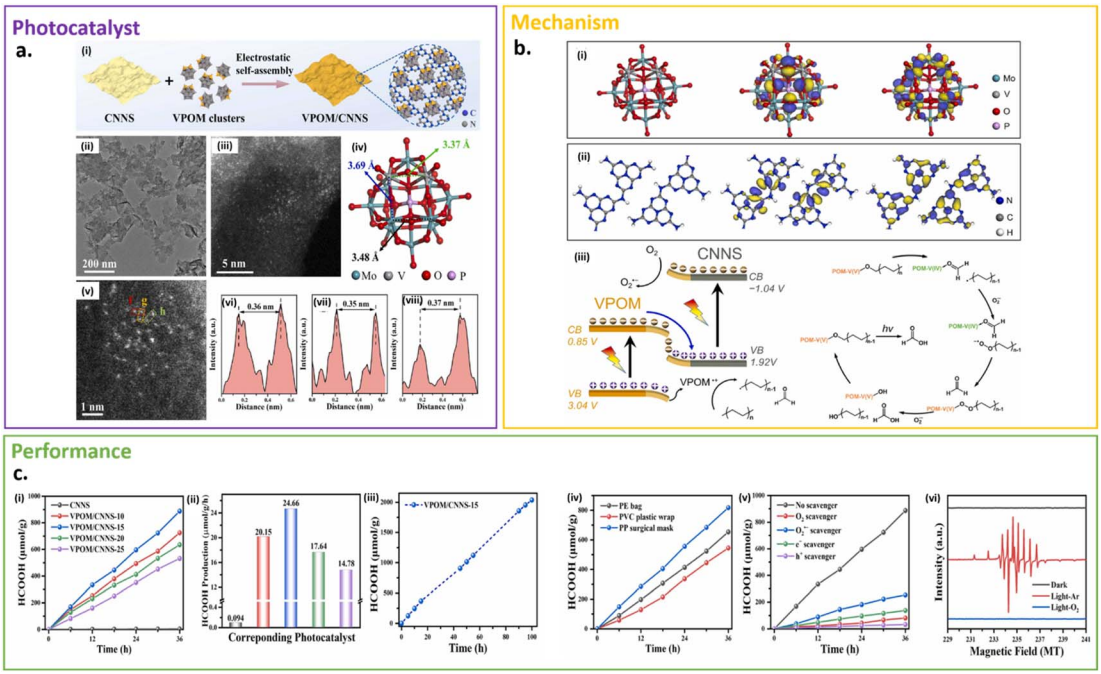

Fig. 9 (a) (i) Schematic diagram of VPOM/CNNS heterojunction prepared *via* electrostatic self-assembly process. (ii) TEM images and (iii) AC-HAADF-STEM image of VPOM/CNNS-15 hybrid. (iv) Optimized model of VPOM cluster by theoretical calculation. (v) AC-HAADF-STEM image of VPOM/CNNS-15 hybrid. (vi), (vii), and (viii) Intensity profile of the selected circled area in (v). (b) DFT calculations for the molecular orbits of (i) VPOM cluster and (ii) CNNS model (the left, middle and right columns represent the ball-and-stick representation, HOMO and LUMO orbits, respectively). (iii) Schematic of the photocatalytic upcycling process for VPOM/CNNS *Z*-scheme heterojunction. (iv) Proposed reaction mechanism for photocatalytic upcycling of plastics by the oxidative C–C bond cleavage with VPOM/CNNS hybrid. (c) (i) Photocatalytic upcycling of polyethylene and (ii) bar chart of HCOOH production rates for 36 h irradiation of samples. (iii) Long-term photocatalytic test of VPOM/CNNS-15 for photocatalytic upcycling of polyethylene. (iv) Photocatalytic upcycling of real-world plastic waste over VPOM/CNNS-15. (v) Photocatalytic upcycling of polyethylene with different scavengers of VPOM/CNNS-15. (vi) ESR spectra of reaction mixtures in different reaction conditions. Reproduced with permission from ref. 115. Copyright 2022, Elsevier.

group also found that methanesulfonic (CH_3SO_3H) and *p*-toluenesulfonic acid monohydrate ($pTsOH \cdot H_2O$) can afford the corresponding products.

3.3. Organic/inorganic hybrid photocatalysts

Many studies in hybrid photocatalysts started with the aim of further utilizing TiO_2 with certain polymers.[118,134] In 2008, Zhao *et al.* studied the solid-phase photodegradation of polyethylene (PE) plastic in ambient air under solar light irradiation.[134] They investigated a copper phthalocyanine (CuPc)-modified TiO_2 (TiO_2/CuPc) photocatalyst and observed the enhancement of photocatalytic degradation of PE over the CuPc-modified TiO_2 composite film. According to the research results of Xu Zhao *et al.*, the weight loss rate for the PE-(TiO_2/CuPc) samples was much higher than that of the PE-TiO_2 sample after 160 h. When the mass ratio of CuPc and TiO_2 was approximately equal to 0.7 wt%, the degradation rate reached its peak, which was around 0.23. Compared with the PE-TiO_2 film, the PE-(TiO_2/CuPc) film had a broader absorption range in the solar spectrum, stronger photovoltage intensity and broader photovoltaic response range.

A photocatalyst with high activity, polypyrrole/TiO_2 (PPy/TiO_2), was prepared *via* sol–gel and emulsion polymerization by Li *et al.* in 2010.[118] After 240 h sunlight irradiation, the weight loss rate of PE-PPy/TiO_2 was 35.4%, which was much higher than that of 11.7% for PPy and 3.2% for TiO_2. By coating the PPy conducting polymer, the crystalline structure of TiO_2 was maintained and the visible light capturing ability of TiO_2 was enhanced, accounting for the highly enhanced photocatalytic activity of PPy/TiO_2.[135] In 2011, Fa *et al.* applied TiO_2 nanoparticle-modified perchlorinated iron(II) phthalocyanine ($FePcCl_{16}$) as a photocatalyst for the photodegradation of a poly(vinyl chloride) (PVC) composite.[119] The $FePcCl_{16}$–TiO_2 composite exhibited a remarkable absorbance in the visible region beyond 400 nm, while blank TiO_2 could only absorb UV light and hardly absorbed light beyond 400 nm. The weight loss rate of the PVC–$FePcCl_{16}$–TiO_2 film reached 50% after 240 h irradiation under UV light, which was much higher than 30% weight loss rate of the PVC–TiO_2 film under the same condition. Under 15 days of solar light irradiation experiment, the weight loss rate of the PVC–$FePcCl_{16}$–TiO_2 film was 81%, which was 80% higher than that of the PVC–TiO_2 film. The PVC–$FePcCl_{16}$–

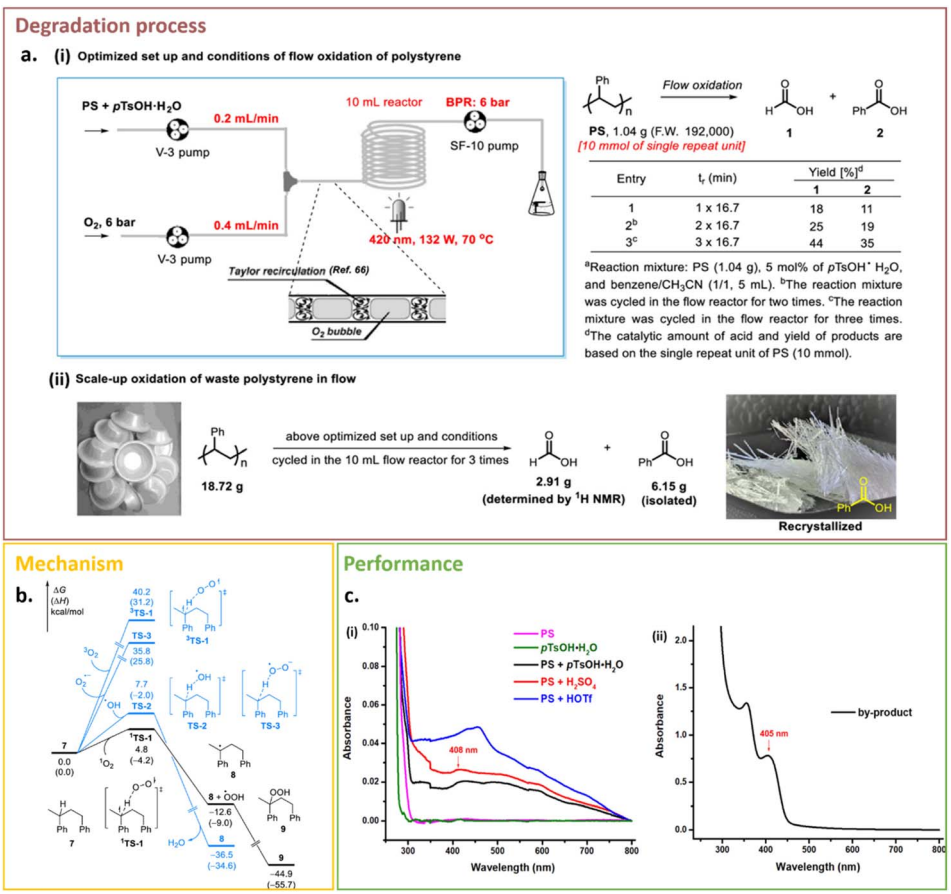

Fig. 10 (a) Computational study of the hydrogen atom transfer (HAT) reaction of 1,3-diphenylbutane 7 with various oxygen species[a] ([a]all energies were calculated at the B3LYP-D3/6-311+G (d,p)/SMD (acetonitrile)//B3LYP-D3/6-31G(d) level of theory). (b) Degradation of PS enabled by photocatalysis in flow: (i) optimized setup and conditions and (ii) gram–scale reaction (note: E-series system from Vapourtec was used for this transformation). (c) UV-vis spectra of PS, $pTsOH \cdot H_2O$, mixture of PS and acid ($pTsOH \cdot H_2O$, H_2SO_4, or HOTf), and the byproduct ([PS]: 10 mM (based on single repeat unit); [acid]: 10 mM; [byproduct]: 1 mg mL^{-1}, in DCE). Reproduced with permission from ref. 133. Copyright 2022, the American Chemical Society.

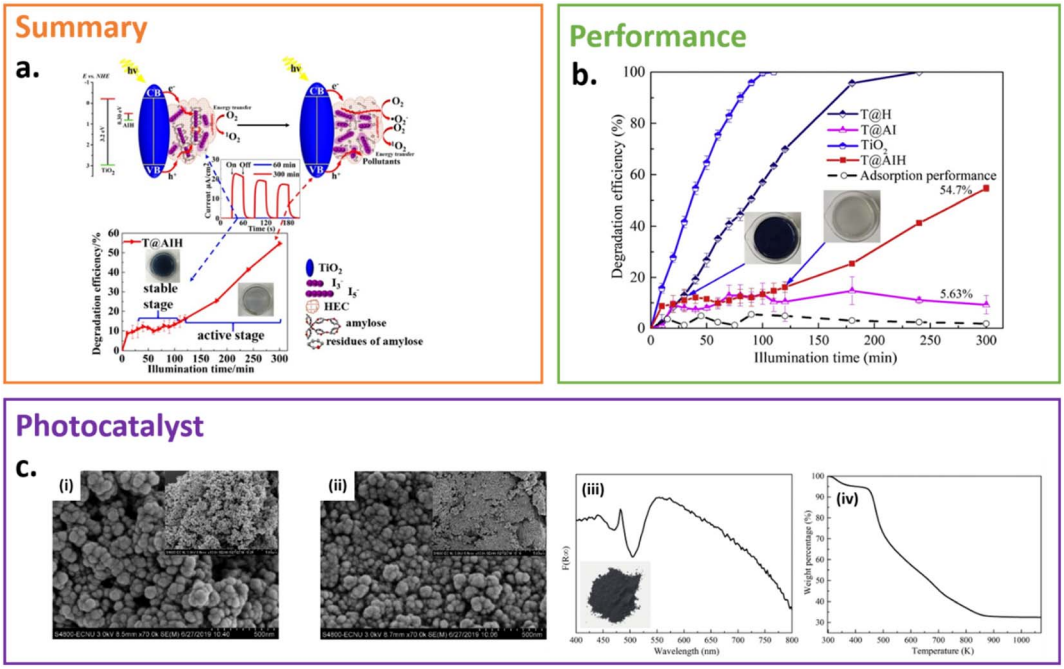

Fig. 11 (a) Photodegradation reaction with newly designed photocatalyst T@AIH. (b) Photocatalytic performance of T@H, T@AI, TiO_2, and T@AIH on phenol degradation and adsorption performance of T@AIH on phenol. (c) SEM images of TiO_2 (i), T@AIH (ii), UV-vis absorption spectrum of T@AIH (iii), and TGA curve of T@AIH (iv). Bottom left inset in (iii) is the digital graph of T@AIH. Reproduced with permission from ref. 78. Copyright 2021, Elsevier.

TiO_2 film showed a higher photodegradation efficiency under both sunlight irradiation and UV light irradiation.

Liang *et al.* prepared a photocatalytic polyacrylamide-grafted TiO_2 (PAM-*g*-TiO_2) nanocomposite and studied the photodegradation of LDPE/PAM-*g*-TiO_2.[120] The weight loss rate of LDPE/TiO_2 was 30.63% under 520 h UV light irradiation. The weight of the LDPE/PAM-TiO_2 composite film decreased by 39.85% under 520 h UV light irradiation and its average molecular weight was reduced by 94.60%. By introducing PAM on TiO_2 particles, good dispersion and hydrophilicity are expected to appear in the LDPE matrix. The reaction between TiO_2 and the adsorbed H_2O in the PAM phase led to an increase in hydroxyl radicals, which initiated the degradation of LDPE.

In 2021, Zhao *et al.* designed a new photocatalyst, TiO_2@-amylose/polyiodide/hydroxyethyl cellulose (T@AIH), for the first time, achieving not only a tunable and stable stage, but encouraging self-colour-changing property and a self-indicating delayed onset of operation (Fig. 11).[78] The particular self-colour-changing property fits well with the beginning of the active stage of degradation, from blue to white, which profits from the addition of hydroxyethyl cellulose (HEC). After 72 h irradiation with the T@$A_{0.1}$IN photocatalyst, LDPE-CP was oxidized, where the carbonyl index (CI) was 0.6556, and mineralized into CO_2. The weight average molecular weight (M_w) of LEPE-CP experienced a reduction from 233 105 g mol^{-1} to 206 370 g mol^{-1}. Similarly, the number average molecular weight (M_n) decreased from 26 234 g mol^{-1} to 1462 g mol^{-1}. The decrease in M_w and M_n indicates the chain breakage reaction of LDPE, suggesting the degradation of the polymer.

Besides TiO_2, C_3N_4 is also commonly employed in the research on hybrid photocatalysts. Sun *et al.* proposed the use of a benzenesulfonyl chloride-incorporated g-C_3N_4 (BS–CN), which is a novel intramolecular donor–acceptor conjugated g-C_3N_4 (Fig. 12).[136] This synthesis extended the π-electron delocalization, narrowing the bandgap and strengthening the absorption in the visible light region, and consequently enhanced the photocatalytic performance significantly. The indirect band gap of CN and BS_5–CN are 2.75 and 2.54 eV, respectively. The grafting of the electron acceptor BS on the CN framework also accelerated the electron transmission and increased the efficiency of the separation of photoexcited electron–hole pairs. Using PLA dispersed in KOH solution as a sacrificial reagent in this work, the H_2 production rate employing Pt-loaded (1 wt%) BS_5–CN was optimized to roughly 1.8-times higher than pure g-C_3N_4, which was 1890 μmol h^{-1} g^{-1} under visible light irradiation, at 40 °C for 24 h. Simultaneously, lactate was oxidized into formate and acetate, achieving the transformation of PLA plastic wastes into high-added-value chemical products and clean hydrogen energy, relieving the environmental pollution and energy dilemma.

In 2022, Han and coworkers focused on carbonized polymer dot-graphitic (CPDs-CN) catalytic solar-driven PET upcycling, together with H_2 production.[137] In this work, PET was used as a valuable feedstock to produce high-value-added products, which were mainly glycolic acid, glycolaldehyde and ethanol, together with H_2 produced from water splitting. The yield of terephthalic acid reached 304.7 ± 17.2 μmol and the production rate of H_2 achieved was 1034 ± 134 μmol g^{-1} h^{-1}, which showed

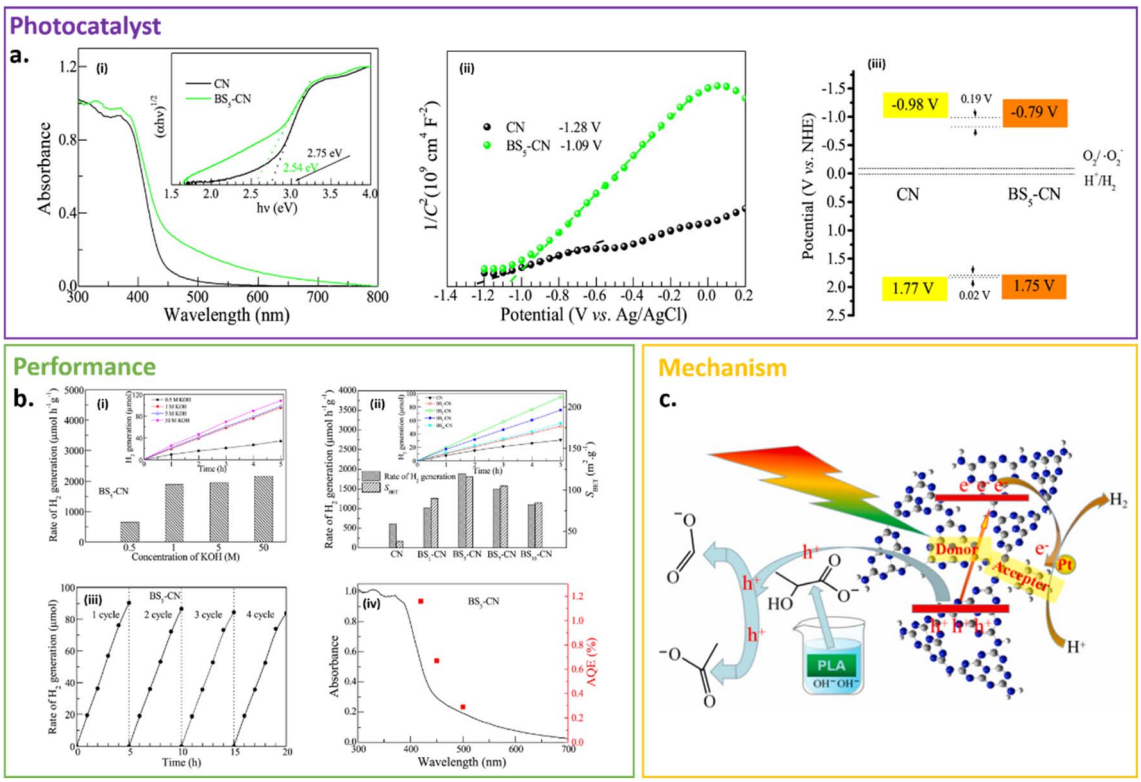

Fig. 12 (a) UV-vis DRS and Tauc plots (i), Mott–Schottky plots (ii), and band position (iii) of CN and BS_5–CN. (b) Effect of the concentration of KOH solution for hydrolysis of PLA with course (inset) and rate of H_2 generation in the presence of BS_5–CN(i), time course (inset) and rate of H_2 production over CN and BS_x-CNs using the hydrolysate of PLA, hydrolyzed in 1 M KOH solution, as the sacrificial reagent, and S_{BET} of CN and BS_x–CNs (ii), photocatalytic stability of BS_5–CN(iii), and AQE of BS_5–CN under three different wavelengths of monochromatic light ($\lambda = 420$, 450, and 500 nm) (iv). (c) Mechanism of photocatalytic production of H_2 and organic chemicals over BS–CN from lactate solution. Reproduced with permission from ref. 136. Copyright 2021, Elsevier.

promising application towards the sustainable production of added-value solar chemicals and fuels.

4. Performance optimization

In this section, we highlight the methods for the optimization and enhancement of the performance for the photocatalytic degradation of plastics. The strategies presented below include the regulation of photocatalysts, the modification of critical intermediates and products during photocatalysis, and the control of environmental factors.

4.1. Regulation of photocatalyst composition

Different types of photocatalysts such as titanium dioxide (TiO_2), zinc oxide (ZnO) and ferric chloride ($FeCI_3$) have been frequently reported thus far.[138] Among them, TiO_2 and ZnO have high catalytic activity and efficiency, and thus have become exceedingly popular.[139,140] However, the use of pure TiO_2 and pure ZnO in photocatalytic degradation still has some limitations. The light absorption edge of pure TiO_2 is lower than 380 nm, and thus most of its current applications are limited to UV light irradiation,[141] while the concentration and dispersion of pure ZnO in the plastic matrix are difficult to regulate,[109] leading to the fact that they cannot be used in their pure form.

Thus, to address this limitation, better photocatalytic efficiency can be obtained by systematically exploring photocatalysts. One of the efficient ways is the combination with other metal/non-metal dopants to enhance the photocatalyst capacity. For example, Asghar *et al.* prepared four types of composite films of PE undoped, Fe-doped, Ag-doped and Fe/Ag mix-doped TiO_2 nanoparticles to research the photocatalytic degradation.[105] The results demonstrated that compared to the PE-TiO_2 films without dopants, the other three composite films showed a more positive effect on weight reduction under the same experimental conditions (Fig. 13a).

Besides, as a result of photodegradation, cavities appeared randomly on the surface of the composite films, which were caused by the escape of volatile products from the PE matrix. It was be observed that the PE-TiO_2 film had massive cavities,[142] while the composite films doped with metal had larger cavities, showing a rough shape (Fig. 13b). This strongly demonstrated that the photocatalytic plastic degradation capability of TiO_2 doped with metals is more efficient than that of undoped TiO_2. In addition, the effect of the mixed doping of the PE-TiO_2 composite film was midway between the Fe-doped and Ag-doped PE-TiO_2 films. This indicated that photocatalysts with some specific requirements can be obtained by adjusting the ratio of doped metal ratios. Similar results were found in the studies by Thomas *et al.*,[143] Zhao *et al.*,[144] and Gonçalves *et al.*[145]

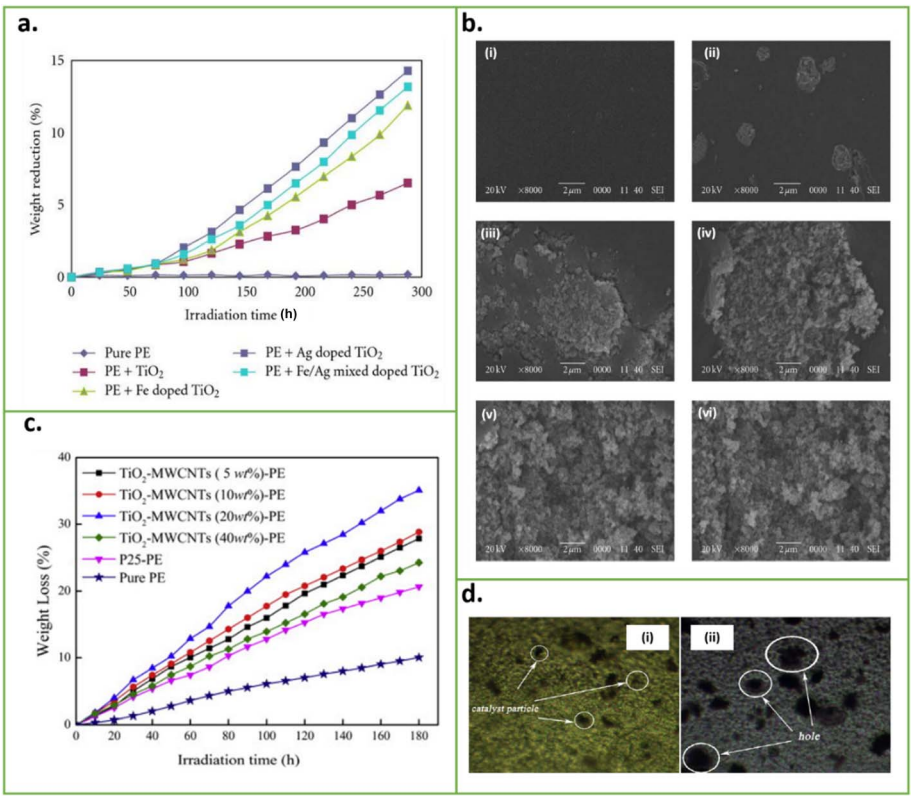

Fig. 13 (a) Effect of UV irradiation on the photocatalytic degradation of PE films. (b) SEM images of PE films before and after irradiation: (i) PE film before irradiation, (ii) PE film after irradiation, (iii) PE-TiO_2 film after irradiation, (iv) PE-Fe doped TiO_2 film after irradiation, (v) PE-Ag-doped TiO_2 film after irradiation, and (vi) PE-Fe/Ag mix-doped TiO_2 film after irradiation. Reproduced with permission from ref. 105. Copyright 2011, Hindawi Publishing Corporation. (c) Weight loss of PE, P25-PE and TiO_2-MWCNT-PE films with different MWCNT contents under UV irradiation in air. (d) Optical microscopy images of the TiO_2-MWCNT (20 wt%)-PE film before (i) and after (ii) irradiation. The objective magnification is 40×. Reproduced with permission from ref. 107. Copyright 2014, Elsevier.

An *et al.* investigated the photocatalytic degradation of TiO_2-MWCNTs-PE films with MWCNT weight contents of 5 wt%, 10 wt%, 20 wt% and 40 wt% by weight loss analysis under mercury lamp irradiation in the ambient air.[107] After 180 h irradiation under identical experiment conditions, the weight reduction of four films with different mass ratios of MWCNTs was 28%, 29%, 35% and 24% respectively, among which the TiO_2-MWCNT (20 wt%)-PE composite film showed the highest photodegradable efficiency (Fig. 13c). Also, the optical microscopic images of the TiO_2-MWCNT (20 wt%)-PE composite film before and after irradiation indicated that assorted sizes of cavities and holes appeared around the photocatalyst particles (Fig. 13d).

As the exposure time prolonged, it was evident that the photodegradation efficiency of the composite films increased with an increase in the MWCNT mass ratio ranging from 5 wt% to 20 wt%, while that for the TiO_2-MWCNT (40 wt%)-PE composite film was the opposite. Their research confirmed that by adjusting the loading of MWCNTs, the optimal photodegradation efficiency could be achieved. Many other studies showed the advantages of MWCNTs, which proposed that they can be used as photosensitizers to broaden the absorption band of TiO_2 to the visible spectrum, thereby improving the efficiency of photocatalysts.[146,147] Moreover, the particle size and morphology of photocatalysts also affect the photocatalytic rate. For instance, Kamrannejad *et al.* studied the factors affecting the photocatalytic degradation behavior of carbon-coated TiO_2 nanotubes in polypropylene (PP)-based nanocomposites, including particle size and thickness of the carbon layer.[148] A thicker carbon layer reduced the penetration of UV light,[149,150] which decreased the photocatalytic efficiency. Also, with an increase in particle size, the interfacial area between PP and the TiO_2 reduced, leading to the lower photocatalytic efficiency.[151]

Besides conventional inorganic semiconductor-based composites photocatalysts, researchers also turned their attention to organic and hybrid photocatalysts.[116,119,120] In the case of organic photocatalysts, the selective addition of acids (sulfuric acid (H_2SO_4), nitric acid (HNO_3), perchloric acid ($HClO_4$), *etc.*) to the reaction process is usually employed to improve the efficiency for the photodegradation of plastics and the yield of recyclable products. These additional acids played a significant role in the oxygen reduction reaction and removing excess H_2O generated during the reaction. Besides, to achieve selective oxidation or cleavage of C–H bonds, hydrogen atom transfer (HAT) catalysts are often added.[152,153] For hybrid photocatalysts, the most important thing is to regulate the concentration of suitable hybridizer, which may reduce the efficiency of photodegradation plastic reaction if it is too high or too low.

4.2. Modification of critical intermediates and products

During the process of the photocatalytic degradation of plastics, the production of some intermediates is inevitable, which may reduce the reaction rate and products, which are difficult to recycle. To make the reaction as environmentally friendly as possible, and eventually upgraded and recycled for human use,[154–156] critical intermediates, clean products (such as water and carbon dioxide) and recyclable products should be obtained through the pretreatment of the reactants and the optimization of the reaction conditions for the photocatalytic degradation reaction. Research has been widely conducted to minimize the pollution to the environment in the reaction process and realize the complete degradation and recycling of plastics.[22,157]

4.2.1. Reactant pretreatment. Most plastics have poor heat resistance and large thermal expansion rate. They are easy to be oxidized if being kept in an elevated temperature environment for a long time. Due to these characteristics, Cao *et al.* researched the degradation characteristics of partially oxidized or relatively soluble precursors obtained by different pretreatments of polystyrene (PS) at different temperatures.[113] Compared with PS, some of these precursors (PS–O, PS-1, PS-2 and PS-3) showed a higher reaction rate and product selectivity in photocatalytic degradation reactions, reflecting the reaction advantages, which made the continuous flow reaction system possible (Fig. 14a).

The pretreatment of plastics seems to be a small step, but it contributes greatly to the improvement of the efficiency and product selectivity of the photocatalytic reaction system.

4.2.2. Reaction conditions adjustment. Many chemical reactions occur during the photocatalytic degradation of plastics. Therefore, the adjustment of the chemical reaction conditions will also affect the degradation reaction rate to a certain extent. Zhang *et al.* reported an alkyl aromatic oxidation directed towards the oxidative degradation of PS into aromatic acids (benzoic acids) catalyzed by $FeCl_3$ and 2,2,2-trichloroethanol (CCl_3CH_2OH) under blue light irradiation and 1 atm O_2 as the sole terminal oxidant at room temperature.[111] According to the plausible mechanism scheme (Fig. 14b), the efficient activation and deep oxidation to carboxylic acid could be achieved by iron-photocatalyst-facilitated selective $C(sp^3)$–$C(sp^3)$ bond cleavage and subsequent oxidation and CCl_3CH_2-OH-facilitated HAT.[111,158–160] The selective cleavage of the $C(sp^3)$–$C(sp^3)$ bonds could convert the polymer into low-weight oligomeric intermediates (tertiary alcohols/peroxides, *etc.*). However, the corresponding intermediates could be deeply oxidized to benzoic acids in the photoinduced iron catalytic system with oxygen molecules. In the whole reaction, the role of molecular

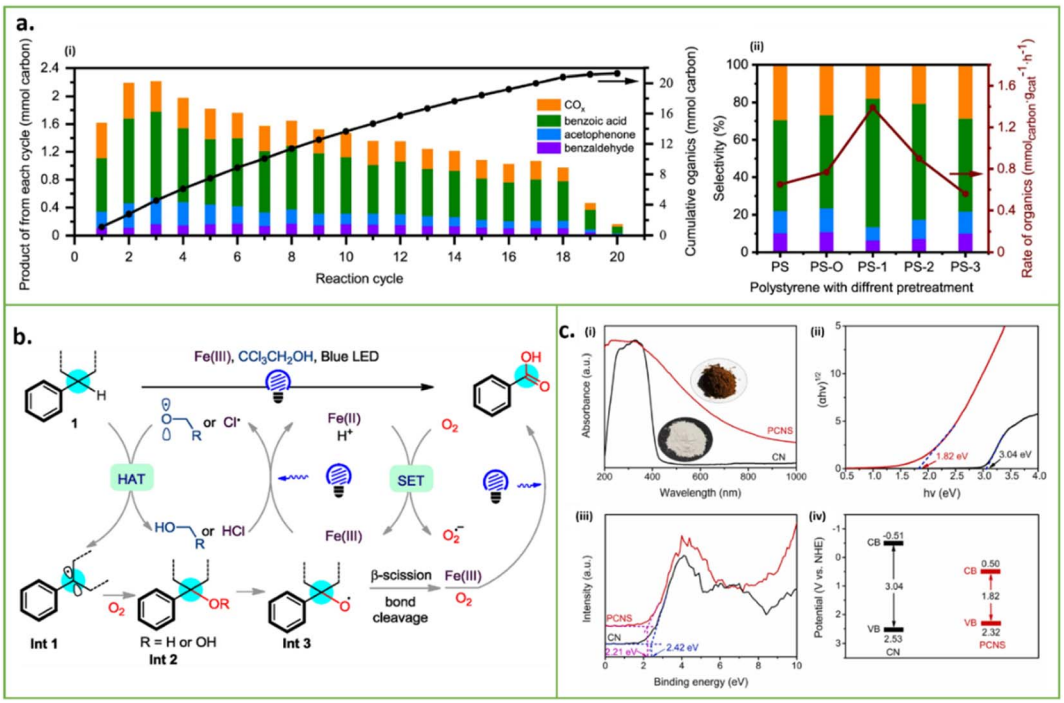

Fig. 14 (a) (i) Conversion of 500 mg plastic pellets in 20 reaction cycles, reaction conditions: 200 mg g-C_3N_4, 500 mg pellets, 40 mL acetonitrile, 10 bar O_2, irradiated by 300 W Xenon lamp at 150 °C for 8 h in each cycle. The solution is released after each cycle and pure solvent is injected in the autoclave. (b) Catalytic performance of polystyrene with different pretreatment, reaction conditions: 50 mg g-C_3N_4, 20 mg polystyrene, 30 mL acetonitrile, irradiated by 300 W Xenon lamp at 150 °C for 8 h. PS-O was obtained by thermal treatment at 150 °C in acetonitrile with O_2, PS-1 and PS-2 were obtained by air treatment at 220 °C and 300 °C, respectively, and PS-3 was obtained by pyrolysis at 350 °C in N_2. Reproduced with permission from ref. 113. Copyright 2022, Springer Nature. (b) Plausible mechanism of the reaction. Reproduced with permission from ref. 111. Copyright 2021, Wiley-VCH. (c) (i) UV-vis absorption spectra of PCNS and CN; the insets show photographs of PCNS and CN. (ii) Plots of transformed Kubelka–Munk function *versus* the energy ($h\nu$) of absorbed light for PCNS and CN. (iii) XPS VB spectra and (iv) band structures of PCNS and CN. Reproduced with permission from ref. 95. Copyright 2022, Elsevier.

oxygen and CCl_3CH_2OH could not be ignored. In fact, in the absence of CCl_3CH_2OH, the reaction product benzoic acid was only slightly produced.

Alternatively, Liu *et al.* engineered a novel carbon nitride (C_3N_4)-based donor–acceptor (D–A) conjugated copolymer.[95] The aromatic ring was incorporated in the C_3N_4 skeleton to form the structure through the copolymerization of melamine and terephthalic acid obtained from the degradation of waste PET catalyzed by ZnO at 360 °C. They prepared PET-derived C_3N_4 sheets (PCNS) and used C_3N_4 (CN) for comparison. Compared with pristine CN, the synthesis of the intramolecular D–A conjugated structure strongly promoted the migration and separation of charge carriers, significantly enhanced the ability of capturing visible light (Fig. 14c) and made the C_3N_4-based D–A conjugated copolymer photocatalysts exhibit better photoinduced charge transfer efficiency. Besides, the special structure greatly narrowed the band gap and enhanced the carrier mobility. These results have been confirmed by many other studies.[161–164] Through the transformation, structure modification and copolymerization of the products during the photodegradation of waste plastics, more efficient photocatalysts can be obtained, which is conductive to the sustainable development and recycling of resources.

The adjustment of reaction conditions involves the use or modification of intermediates and products to achieve the more efficient photocatalytic degradation of plastics or recycling

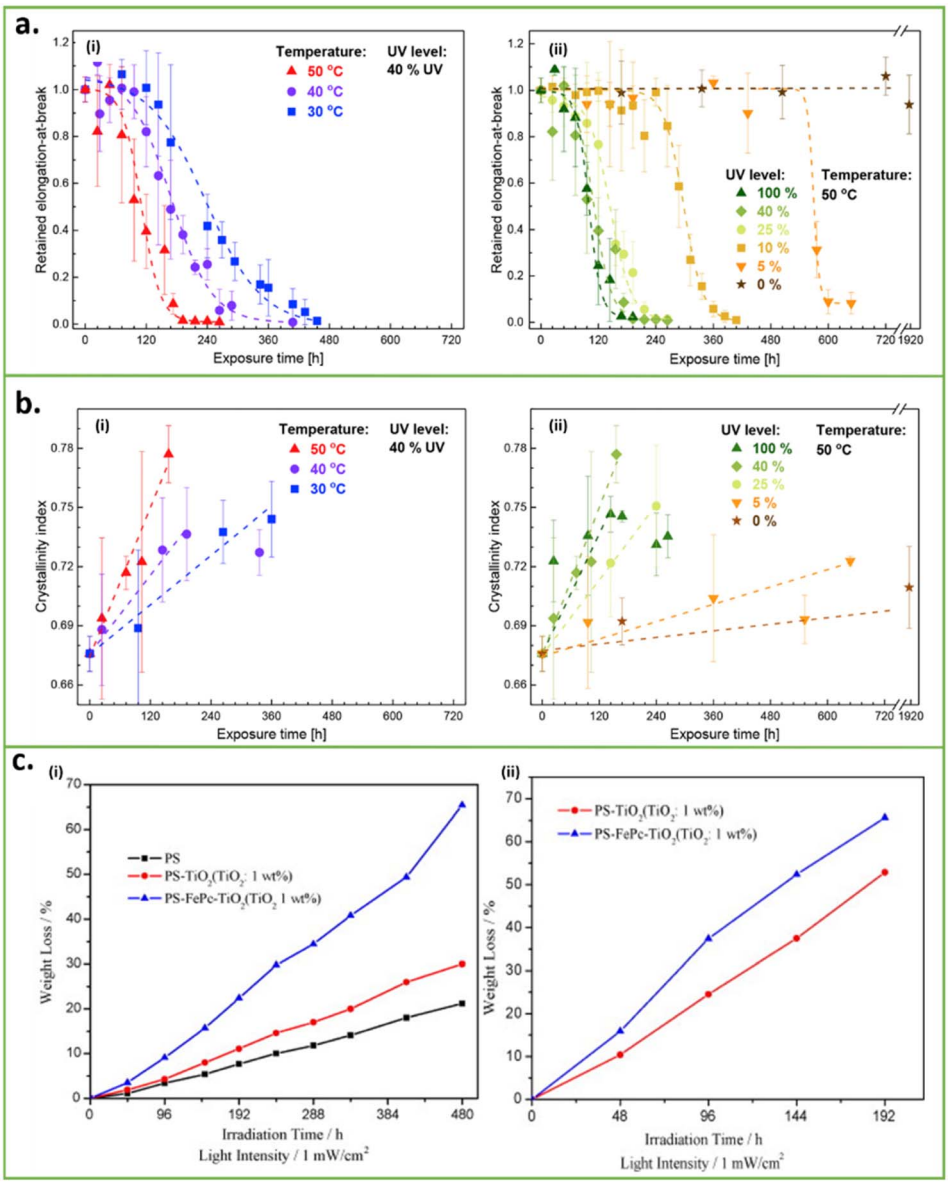

Fig. 15 (a) Retained elongation-at-break as a function of exposure time (i) at 30 °C, 40 °C, and 50 °C with 40% UV irradiance and (ii) at 50 °C with 0%, 5%, 10%, 25%, 40%, and 100% UV irradiance. (b) Surface crystallinity index for HDPE as a function of exposure time (i) at 30 °C, 40 °C, and 50 °C with 40% UV irradiance and (ii) at 50 °C with 0%, 5%, 10%, 25%, 40%, and 100% UV irradiance. Reproduced with permission from ref. 96. Copyright 2019, Elsevier. (c) Weight loss of the composite films under UV light irradiation in (i) dry air and (ii) humidified air. Reproduced with permission from ref. 103. Copyright 2008, Elsevier.

plastic waste for industrial manufacturing, which is killing two birds with one stone.

4.3. Control of environmental factors

In previous studies, most of the experiments were carried out under a single laboratory condition,[165] which remained fixed and stable for a long time. Benefitting from this, the plastic degradation rate was smoothly sustained. In contrast, during actual outdoor photocatalytic degradation, the light intensity, temperature and humidity randomly change with the weather conditions.[166] Therefore, the control of environmental factors cannot be neglected in the experimental processes for the photocatalytic degradation of plastics.

Fairbrother *et al.* investigated the effects of environmental factors on the performance of photodegradable high-density polyethylene (HDPE) under a range of laboratory conditions, including three temperature levels (30 °C, 40 °C, and 50 °C), six UV irradiation levels from a metal halide light source (153 W m^{-2}, 61 W m^{-2}, 38 W m^{-2}, 15 W m^{-2}, 8 W m^{-2} and 0 W m^{-2}) and two humidity conditions (<5% relative humidity (RH) and 75% RH).[96] According to the results, an increase in temperature and UV intensity tended to accelerate the change of the mechanical properties of HDPE. The retained elongation-at-break of HDPE under harsher conditions with the same exposure time was larger, and the change rate of mechanical properties was faster (Fig. 15a), and thus the surface crystallinity index for HEDP (Fig. 15b). The overall conclusions were consistent with that in other reports.[167–170] Nevertheless, there was no significant difference between the two humidity conditions for HDPE, possibly because of its high hydrophobicity.

Similarly, they left HDPE exposed outdoors in southern Florida in the United States and examined it periodically during exposure to quantify the effect of each environmental factors on the photodegradation on HDPE through the change in performance. In this case, outdoor conditions are more diverse and complicated, making it difficult to compare with the laboratory environment. Under outdoor exposure conditions, the brittle failure time was over two times longer than that under accelerated laboratory conditions. The rate of performance change outdoors did not easily match that seen in the laboratory due to the spectral differences and cyclic changes in the outdoor environment. Up to the end of the exposure period, the variation in mechanical properties well matched the variation in laboratory exposure at 40 °C and 50 °C.

The values of retained elongation-at-break, yield stress, modulus of elasticity and crystallinity indices outdoors were close to that at 40% UV exposure in the laboratory experiment at the two higher temperatures studied. The fact that the mechanical properties measured at embrittlement matched the values under laboratory conditions positively implied that the photodegradation pathway is similar in the laboratory and outdoor environment.

Furthermore, Fa *et al.* revealed the effect of water vapor of a novel photodegradable PS–FePc–TiO_2 nanocomposite film under humidified air and dry air.[103] The weight loss of the composite film was greater in a higher humidity environment, whereas it was only one-third of that in dry air (Fig. 15c). This proposed the physical adsorption of a certain amount of water is essential for the photodegradation of PS films. These conclusions were also similar to that in other reports.[171–173]

In most scenarios, plastic is treated as household waste and pollution. Consequently, to realize the wide practical application of the photocatalytic degradation of plastics, the influence of environmental factors should be considered.

5. Conclusions and future perspectives

With the improvement in the awareness of protecting the environment, unprecedented efforts have been devoted to exploring novel and effective ways of degrading plastics for their disposal, among which photocatalysis is a method with great prospects. In this review, we systematically summarized various reports in the literature concerning photocatalysis and the different categories of photocatalysts, ranging from typical bare semiconductors such as TiO_2, ZnO, and MnO to composite inorganic materials, organic materials and hybrid materials. Then, we list some remaining aspects that were analysed to be influential on the catalytic efficiency, benefiting the further optimization process of photocatalysis. However, the fact that the current degradation rate of plastics remains unchanged at less than 10%, pervasive microplastics pose an ongoing threat to all animals, plants and humans on Earth. To date, photocatalysis is still at the initial theoretical stage and we need steps forward. Here, we list some limitations and potential development prospects, which may favour an enhancement in the possibility of practical applications and are worthwhile to research more comprehensively:

5.1. Photocatalyst upgrade

Semiconductors including metal sulfides, phosphides, nitrides and oxides[31] make up a large proportion of the present research in photocatalyst materials. However, although they exhibit good performances in photocatalysis experiments, the high costs of their raw materials and manufacture have impeded their large-scale application. This is the same for composite, organic and hybrid photocatalysts. Furthermore, during the degradation, photocatalysts are treated at the nanoscale, resulting in pollution and nanotoxicity and damaging the ecological environment. Besides this potential detriment, the modification of photocatalysts on plastics is still conducted at the laboratory scale, which may not be achieved industrially. Therefore, new types of light-sensitive materials should be explored with properties such as low price, low pollution, high effectiveness and high product selectivity. Techniques involving cocatalyst deposition, heteroatom doping, heterostructure construction and defect engineering[30] can be attempted simultaneously to upgrade the nature of photocatalysts.

5.2. Extension and pretreatment of plastics

Most plastics that are given attention are confined to commercial plastics, while engineering plastics are largely neglected.

More types of plastics should be considered, which also cause severe white pollution. Next, before the degradation of plastics, they require pretreatment, where plastics are dissolved in a certain solvent by regulating the pH level, mostly in the alkaline range. On the one hand, alkaline reagents will be rarely harmful to the environment if they are treated inappropriately. On the other hand, pretreatment increases the degradation cost, slowing down the commercial realization of photocatalysis. Besides, experiments only consider the ideal case of a single polymer component. Nevertheless, in the real world, plastics are composed of numerous complex components, containing complicated impurities and defects. These compositions may be obstructions towards the degradation efficiency and rate, triggering a huge gap between experimental results and actual application. Thus, experiments based on real-life plastics should be conducted to examine whether photocatalysts can work to degrade complex polymer components.

5.3. Product utilization

Thus far, the majority of the intermediates and final products from the photocatalytic degradation of plastics are low molecular weight organic matter, CO_2 and H_2, which are of great use in certain chemical fields. However, CO_2 is one of the well-known greenhouse gases and when emitted directly to the atmosphere through the degradation of plastics, it can lead to the severe greenhouse effect and contribute to global warming. Similarly, although organic products can be applied some way, their toxicity to organisms and pollution of the surroundings cannot be neglected, which can be easily abused and result in critical problems such as water pollution. Also, considering the uncertainty of the reaction process, side reactions can occur and their products are unknown. Consequently, consecutive studies aimed at product utilization should be conducted to eliminate the negative effects of products to the greatest extent.

5.4. Applicability at the commercial scale

The subsistent problems are much more complex than the experiment, and there are many obstacles in the process of the large-scale promotion of photocatalysis. Firstly, current techniques cannot eliminate the microplastics in the soil and ocean, which requires more studies about the reaction mechanisms to determine more possible ways to achieve photocatalysis. Secondly, degradation techniques need to be optimized, especially to reduce the costs of the entire disposal process. Practical usage necessitates commercial interest, and to substitute conventional indispensable plastics, a relatively low price is essential. Thirdly, to show the high degradation efficiency of photocatalysis, most studies use UV light as the energy source. However, when exploiting it in reality, there is 4% of UV light in sunlight, which will largely retard the degradation rate. Hence, on account of controlling the cost, researchers can try to improve the efficiency by applying electric or magnetic fields, increasing the temperature or pressure.

Briefly, the optimization of the photocatalytic degradation of plastics requires the overall improvement of photocatalysts, reactors and reaction media. To realize the overall disposal of plastics and microplastics through photocatalysis, more research should be conducted to achieve commercial success, together with the technique being suitable for mass manufacture. Moreover, great physical and mechanical properties corresponding to typical plastics should also be achieved based on environmental protection. Accordingly, photocatalysis can become widespread and gradually replace conventional plastics or conservative strategies of disposing plastics. Photocatalysis is quite promising in degrading plastics and we believe that it can be widely applied one day.

Conflicts of interest

There are no conflicts to declare.

Acknowledgements

This study was financially supported by the Program for the Natural Science Foundation of Shaanxi Province, China (2021JM-052), and the Fundamental Research Funds for the Central Universities (0201021GH0201, 0206022SH0201).

References

1 J. Watts, *The Guardian*, 2019, vol. 25, pp. 1–9.
2 G. Maitlo, I. Ali, H. A. Maitlo, S. Ali, I. N. Unar, M. B. Ahmad, D. K. Bhutto, R. K. Karmani, S. u. R. Naich and R. U. Sajjad, *Sustainability*, 2022, **14**, 11637.
3 M. U. Hossain, S. T. Ng, Y. Dong and B. Amor, *Waste Manage.*, 2021, **131**, 412–422.
4 M. Williams, R. Gower, J. Green, E. Whitebread, Z. Lenkiewicz and P. Schröder, *No Time to Waste: Tackling the Plastic Pollution Crisis before It's Too Late*, 2019.
5 T. Maes, J. McGlade, I. S. Fahim, D. S. Green, P. Landrigan, A. L. Andrady, M. F. Costa, R. Geyer, R. Gomes and A. T. S. Hwai, *From Pollution to Solution: A Global Assessment of Marine Litter and Plastic Pollution*, Report 928073881X, 2021.
6 F. Sadeghfar and M. Ghaedi, in *Interface Science and Technology*, Elsevier, 2021, vol. 32, pp. 725–759.
7 P. J. Kole, A. J. Löhr, F. G. Van Belleghem and A. M. Ragas, *Int. J. Environ. Res. Public Health*, 2017, **14**, 1265.
8 J. Zheng and S. Suh, *Nat. Clim. Change*, 2019, **9**, 374–378.
9 A. Demetrious and E. Crossin, *J. Mater. Cycles Waste Manage.*, 2019, **21**, 850–860.
10 B. K. Guptaa and S. Singhb, *Int. J. Appl. Eng. Res.*, 2018, **13**, 5815–5822.
11 G. Suzuki, N. Uchida, K. Tanaka, H. Matsukami, T. Kunisue, S. Takahashi, P. H. Viet, H. Kuramochi and M. Osako, *Environ. Pollut.*, 2022, **303**, 119114.
12 A. D. Vethaak and J. Legler, *Science*, 2021, **371**, 672–674.
13 H. Luo, D. Yao, K. Zeng, J. Li, S. Yan, D. Zhong, J. Hu, H. Yang and H. Chen, *Fuel Process. Technol.*, 2022, **230**, 107205.
14 K. Zhang, A. H. Hamidian, A. Tubić, Y. Zhang, J. K. Fang, C. Wu and P. K. Lam, *Environ. Pollut.*, 2021, **274**, 116554.

15 X. Zhao, M. Korey, K. Li, K. Copenhaver, H. Tekinalp, S. Celik, K. Kalaitzidou, R. Ruan, A. J. Ragauskas and S. Ozcan, *Chem. Eng. J.*, 2022, **428**, 131928.
16 E. Bäckström, K. Odelius and M. Hakkarainen, *Ind. Eng. Chem. Res.*, 2017, **56**, 14814–14821.
17 C. De Monte, M. Locritani, S. Merlino, L. Ricci, A. Pistolesi and S. Bronco, *Polymers*, 2022, **14**, 1111.
18 L. Tang, H. Huang, Z. Zhao, C. Wu and Y. Chen, *Ind. Eng. Chem. Res.*, 2003, **42**, 1145–1150.
19 M. V. Navarro, J. D. Martínez, R. Murillo, T. García, J. M. López, M. S. Callén and A. M. Mastral, *Fuel Process. Technol.*, 2012, **103**, 1–8.
20 X. Gong, F. Tong, F. Ma, Y. Zhang, P. Zhou, Z. Wang, Y. Liu, P. Wang, H. Cheng and Y. Dai, *Appl. Catal., B*, 2022, **307**, 121143.
21 J. Ge, Z. Zhang, Z. Ouyang, M. Shang, P. Liu, H. Li and X. Guo, *Environ. Res.*, 2022, **209**, 112729.
22 S. Chu, B. Zhang, X. Zhao, H. S. Soo, F. Wang, R. Xiao and H. Zhang, *Adv. Energy Mater.*, 2022, **12**, 2200435.
23 V. Lad and Z. Murthy, in *Handbook of Smart Photocatalytic Materials*, Elsevier, 2020, pp. 3–8.
24 R. P. Barkul, M. K. Patil, S. M. Patil, V. B. Shevale and S. D. Delekar, *J. Photochem. Photobiol., A*, 2017, **349**, 138–147.
25 K. Hu, Y. Yang, Y. Wang, X. Duan and S. Wang, *Chem Catal.*, 2022, **2**, 724–761.
26 Q. Guo, C. Zhou, Z. Ma and X. Yang, *Adv. Mater.*, 2019, **31**, 1901997.
27 C. Hu, M. Zhao, Q. Li, Z. Liu, N. Hao, X. Meng, J. Li, F. Lin, C. Li, L. Fang, S. Y. Dai, A. J. Ragauskas, H. J. Sue and J. S. Yuan, *ChemSusChem*, 2021, **14**, 4260–4269.
28 Q. Y. Lee and H. Li, *Micromachines*, 2021, **12**, 907.
29 P. Ebrahimbabaie, K. Yousefi and J. Pichtel, *Sci. Total Environ.*, 2022, **806**, 150603.
30 M. Du, M. Xing, S. Kang, Y. Ma, B. Qiu and Y. Chai, *EcoMat*, 2022, e12259.
31 A. Chen, M.-Q. Yang, S. Wang and Q. Qian, *Front. Nanotechnol.*, 2021, **3**, 723120.
32 D. Castilla-Caballero, O. Sadak, J. Martínez-Díaz, V. Martínez-Castro, J. Colina-Márquez, F. Machuca-Martínez, A. Hernandez-Ramirez, S. Vazquez-Rodriguez and S. Gunasekaran, *Mater. Sci. Semicond. Process.*, 2022, **149**, 106890.
33 M. R. Karimi Estahbanati, X. Y. Kong, A. Eslami and H. S. Soo, *ChemSusChem*, 2021, **14**, 4152–4166.
34 K. Zheng, Y. Wu, Z. Hu, S. Wang, X. Jiao, J. Zhu, Y. Sun and Y. Xie, *Chem. Soc. Rev.*, 2023, **52**, 8–29.
35 C. Zhang, Q. Kang, M. Chu, L. He and J. Chen, *TrAC, Trends Anal. Chem.*, 2022, **4**, 822–834.
36 M. Chu, Y. Liu, X. Lou, Q. Zhang and J. Chen, *ACS Catal.*, 2022, **12**, 4659–4679.
37 K. Enders, R. Lenz, S. Beer and C. A. Stedmon, *ICES J. Mar. Sci.*, 2017, **74**, 326–331.
38 A. Adeniyi, O. Agboola, E. R. Sadiku, M. Durowoju, P. Olubambi, A. B. Reddy, I. Ibrahim and W. Kupolati, in *Design and Applications of Nanostructured Polymer Blends and Nanocomposite Systems*, Elsevier, 2016, pp. 15–38.
39 E. Bagherpour, N. Pardis, M. Reihanian and R. Ebrahimi, *Int. J. Adv. Des. Manuf. Technol.*, 2019, **100**, 1647–1694.
40 V. Chauhan, T. Kärki and J. Varis, *J. Thermoplast. Compos. Mater.*, 2022, **35**, 1169–1209.
41 S. Abeysinghe, C. Gunasekara, C. Bandara, K. Nguyen, R. Dissanayake and P. Mendis, *Polymers*, 2021, **13**, 1885.
42 A. Shebani, A. Klash, R. Elhabishi, S. Abdsalam, H. Elbreki and W. Elhrari, *Res. Dev. Mater. Sci.*, 2018, **7**, 791–797.
43 K. Sterky, H. Jacobsen, I. Jakubowicz, N. Yarahmadi and T. Hjertberg, *Eur. Polym. J.*, 2010, **46**, 1203–1209.
44 H. Ebadi-Dehaghani, H. A. Khonakdar, M. Barikani and S. H. Jafari, *Composites, Part B*, 2015, **69**, 133–144.
45 B. A. Ibrahim and K. M. Kadum, *Int. J. Eng. Sci.*, 2012, **12**, 19–27.
46 M. R. Havstad, in *Plastic Waste and Recycling*, Elsevier, 2020, pp. 97–129.
47 M. Rujnić-Sokele and A. Pilipović, *Waste Manage. Res.*, 2017, **35**, 132–140.
48 E. Dilshad, H. Waheed, U. Ali, A. Amin and I. Ahmed, in *Bioplastics for Sustainable Development*, Springer, 2021, pp. 61–82.
49 J. Butt, P. Oxford, S. Sadeghi-Esfahlani, M. Ghorabian and H. Shirvani, *Arabian J. Sci. Eng.*, 2020, **45**, 9339–9356.
50 S. Jiang, Y. Yang, S. Ge, Z. Zhang and W. Peng, *Arabian J. Chem.*, 2018, **11**, 844–857.
51 J. Jian, Z. Xiangbin and H. Xianbo, *Adv. Ind. Eng. Polym. Res.*, 2020, **3**, 19–26.
52 Y. Zhao, G. Chen, M. Xiao, S. Wang and Y. Meng, *J. Polym. Res.*, 2016, **23**, 1–10.
53 S. Wachirahuttapong, C. Thongpin and N. Sombatsompop, *Energy Procedia*, 2016, **89**, 198–206.
54 E. Ten, L. Jiang, J. Zhang and M. Wolcott, *Biocomposites*, 2015, 39–52.
55 Y. J. Low, A. Andriyana, B. C. Ang and N. I. Zainal Abidin, *Polym. Eng. Sci.*, 2020, **60**, 2657–2675.
56 T. D. Moshood, G. Nawanir, F. Mahmud, F. Mohamad, M. H. Ahmad and A. AbdulGhani, *Curr. Res. Green Sustainable Chem.*, 2022, 100273.
57 D. G. Hayes, L. C. Wadsworth, H. Y. Sintim, M. Flury, M. English, S. Schaeffer and A. M. Saxton, *Polym. Test.*, 2017, **62**, 454–467.
58 M. Shen, B. Song, G. Zeng, Y. Zhang, W. Huang, X. Wen and W. Tang, *Environ. Pollut.*, 2020, **263**, 114469.
59 R. C. Hale, M. E. Seeley, M. J. La Guardia, L. Mai and E. Y. Zeng, *J. Geophys. Res.: Oceans*, 2020, **125**, e2018JC014719.
60 C. Wang, J. Zhao and B. Xing, *J. Hazard. Mater.*, 2021, **407**, 124357.
61 O. Bajt, *FEBS Open Bio*, 2021, **11**, 954–966.
62 L. Van Cauwenberghe and C. R. Janssen, *Environ. Pollut.*, 2014, **193**, 65–70.
63 A. K. Baldwin, S. R. Corsi and S. A. Mason, *Environ. Sci. Technol.*, 2016, **50**, 10377–10385.
64 R. A. Castañeda, S. Avlijas, M. A. Simard and A. Ricciardi, *Can. J. Fish. Aquat. Sci.*, 2014, **71**, 1767–1771.

65 M. Eriksen, S. Mason, S. Wilson, C. Box, A. Zellers, W. Edwards, H. Farley and S. Amato, *Mar. Pollut. Bull.*, 2013, **77**, 177–182.
66 W. Sanchez, C. Bender and J.-M. Porcher, *Environ. Res.*, 2014, **128**, 98–100.
67 A. H. Anik, S. Hossain, M. Alam, M. B. Sultan, M. T. Hasnine and M. M. Rahman, *Environ. Nanotechnol., Monit. Manage.*, 2021, **16**, 100530.
68 A. K. Mishra, J. Singh and P. P. Mishra, *Sci. Total Environ.*, 2021, **784**, 147149.
69 D. A. Strifling, *J. land use environ. law*, 2016, **32**, 151–166.
70 N. Brennholt, M. Heß and G. Reifferscheid, in *Freshwater Microplastics*, Springer, Cham, 2018, pp. 239–272.
71 P. Ludlow, in *The New European Community*, Routledge, 2018, pp. 85–132.
72 M. Malankowska, C. Echaide-Gorriz and J. Coronas, *Environ. Sci.: Water Res. Technol.*, 2021, **7**, 243–258.
73 N. Laskar and U. Kumar, *Environ. Technol. Innovation*, 2019, **14**, 100352.
74 J. Yuan, J. Ma, Y. Sun, T. Zhou, Y. Zhao and F. Yu, *Sci. Total Environ.*, 2020, **715**, 136968.
75 J. Wang, X. Liu, Y. Li, T. Powell, X. Wang, G. Wang and P. Zhang, *Sci. Total Environ.*, 2019, **691**, 848–857.
76 B. G. Ranby and J. F. Rabek, *Photodegradation, Photo-Oxidation, and Photostabilization of Polymers*, Wiley, New York, 1975.
77 A. C. Vivekanand, S. Mohapatra and V. K. Tyagi, *Chemosphere*, 2021, **282**, 131151.
78 Y. Zhao, F. Zhang, J. Zhang, K. Zou, J. Zhang, C. Chen, M. Long, Q. Zhang, J. Wang and C. Zheng, *Appl. Catal., B*, 2021, **286**, 119918.
79 B. Qiu, Y. Deng, Q. Li, B. Shen, M. Xing and J. Zhang, *J. Phys. Chem. C*, 2016, **120**, 12125–12131.
80 C. Sanjayan, M. Jyothi and R. G. Balakrishna, *J. Mater. Chem. C*, 2022, **10**, 6935–6956.
81 J. Chen, Z. He, Y. Ji, G. Li, T. An and W. Choi, *Appl. Catal., B*, 2019, **257**, 117912.
82 C. Hu, L. Zhang and J. Gong, *Energy Environ. Sci.*, 2019, **12**, 2620–2645.
83 H. Luo, Y. Xiang, T. Tian and X. Pan, *Sci. Total Environ.*, 2021, **757**, 143900.
84 J. Shang, M. Chai and Y. Zhu, *Environ. Sci. Technol.*, 2003, **37**, 4494–4499.
85 J. Shang, M. Chai and Y. Zhu, *J. Solid State Chem.*, 2003, **174**, 104–110.
86 R. Gusain, K. Gupta, P. Joshi and O. P. Khatri, *Adv. Colloid Interface Sci.*, 2019, **272**, 102009.
87 M. R. Hoffmann, S. T. Martin, W. Choi and D. W. Bahnemann, *Chem. Rev.*, 1995, **95**, 69–96.
88 K. Takanabe and S. Shahid, *AIChE J.*, 2017, **63**, 105–110.
89 M. Melchionna and P. Fornasiero, *ACS Catal.*, 2020, **10**, 5493–5501.
90 K. F. Chin, M. Đokić and H. S. Soo, *TrAC, Trends Anal. Chem.*, 2020, **2**, 485–488.
91 V. Emel'Yanenko, S. Verevkin, C. Schick, E. Stepurko, G. Roganov and M. Georgieva, *Russ. J. Phys. Chem. A*, 2010, **84**, 1491–1497.
92 M. F. Kuehnel and E. Reisner, *Angew. Chem., Int. Ed.*, 2018, **57**, 3290–3296.
93 X. Gong, F. Tong, F. Ma, Y. Zhang, P. Zhou, Z. Wang, Y. Liu, P. Wang, H. Cheng, Y. Dai, Z. Zheng and B. Huang, *Appl. Catal., B*, 2022, **307**, 121143.
94 C. Xing, G. Yu, T. Chen, S. Liu, Q. Sun, Q. Liu, Y. Hu, H. Liu and X. Li, *Appl. Catal., B*, 2021, **298**, 120534.
95 N. Liu, Z. Hu, L. Hao, H. Bai, P. He, R. Niu and J. Gong, *J. Environ. Chem. Eng.*, 2022, **10**, 106959.
96 A. Fairbrother, H.-C. Hsueh, J. H. Kim, D. Jacobs, L. Perry, D. Goodwin, C. White, S. Watson and L.-P. Sung, *Polym. Degrad. Stab.*, 2019, **165**, 153–160.
97 J. F. Heacock, F. B. Mallory and F. P. Gay, *J. Polym. Sci., Part A: Polym. Chem.*, 1968, **6**, 2921–2934.
98 M. Carvalho and J. Cruz-Pinto, *Polym. Eng. Sci.*, 1992, **32**, 567–572.
99 J. Cruz-Pinto, M. Carvalho and J. Ferreira, *Angew. Makromol. Chem.*, 1994, **216**, 113–133.
100 T. Uekert, H. Kasap and E. Reisner, *J. Am. Chem. Soc.*, 2019, **141**, 15201–15210.
101 C. Y. Toe, C. Tsounis, J. Zhang, H. Masood, D. Gunawan, J. Scott and R. Amal, *Energy Environ. Sci.*, 2021, **14**, 1140–1175.
102 S.-Y. Lee, J.-H. Yoon, J.-R. Kim and D.-W. Park, *J. Anal. Appl. Pyrolysis*, 2002, **64**, 71–83.
103 W. Fa, L. Zan, C. Gong, J. Zhong and K. Deng, *Appl. Catal., B*, 2008, **79**, 216–223.
104 S. Cho and W. Choi, *J. Photochem. Photobiol., A*, 2001, **143**, 221–228.
105 W. Asghar, I. A. Qazi, H. Ilyas, A. A. Khan, M. A. Awan and M. Rizwan Aslam, *J. Nanomater.*, 2011, **2011**, 461930.
106 C. Yang, K. Deng, T. Peng and L. Zan, *Chem. Eng. Technol.*, 2011, **34**, 886–892.
107 Y. An, J. Hou, Z. Liu and B. Peng, *Mater. Chem. Phys.*, 2014, **148**, 387–394.
108 G. Liu, S. Liao, D. Zhu, J. Cui and W. Zhou, *Solid State Sci.*, 2011, **13**, 88–94.
109 A. Bandyopadhyay and G. C. Basak, *Mater. Sci. Technol.*, 2007, **23**, 307–314.
110 G. Liu, D. Zhu, W. Zhou, S. Liao, J. Cui, K. Wu and D. Hamilton, *Appl. Surf. Sci.*, 2010, **256**, 2546–2551.
111 G. Zhang, Z. Zhang and R. Zeng, *Chin. J. Chem.*, 2021, **39**, 3225–3230.
112 M. Wang, J. Wen, Y. Huang and P. Hu, *ChemSusChem*, 2021, **14**, 5049–5056.
113 R. Cao, M.-Q. Zhang, C. Hu, D. Xiao, M. Wang and D. Ma, *Nat. Commun.*, 2022, **13**, 4809.
114 T. Uekert, M. F. Kuehnel, D. W. Wakerley and E. Reisner, *Energy Environ. Sci.*, 2018, **11**, 2853–2857.
115 C. Xing, G. Yu, J. Zhou, Q. Liu, T. Chen, H. Liu and X. Li, *Appl. Catal., B*, 2022, **315**, 121496.
116 T. Li, A. Vijeta, C. Casadevall, A. S. Gentleman, T. Euser and E. Reisner, *ACS Catal.*, 2022, **12**, 8155–8163.
117 Z. Huang, M. Shanmugam, Z. Liu, A. Brookfield, E. L. Bennett, R. Guan, D. E. Vega Herrera, J. A. Lopez-Sanchez, A. G. Slater, E. J. L. McInnes, X. Qi and J. Xiao, *J. Am. Chem. Soc.*, 2022, **144**, 6532–6542.

118 S. Li, S. Xu, L. He, F. Xu, Y. Wang and L. Zhang, *Polym.-Plast. Technol. Eng.*, 2010, **49**, 400–406.
119 W. Fa, C. Gong, L. Tian, T. Peng and L. Zan, *J. Appl. Polym. Sci.*, 2011, **122**, 1823–1828.
120 W. Liang, Y. Luo, S. Song, X. Dong and X. Yu, *Polym. Degrad. Stab.*, 2013, **98**, 1754–1761.
121 N. S. Allen, J. F. McKellar, G. O. Phillips and D. G. M. Wood, *J. Polym. Sci., Polym. Lett. Ed.*, 1974, **12**, 241–245.
122 X. Jiao, K. Zheng, Q. Chen, X. Li, Y. Li, W. Shao, J. Xu, J. Zhu, Y. Pan and Y. Sun, *Angew. Chem., Int. Ed.*, 2020, **59**, 15497–15501.
123 S. Oh and E. E. Stache, *J. Am. Chem. Soc.*, 2022, **144**, 5745–5749.
124 M. Hoffman, S. Martin, W. Choi and D. Bahnemann, *Chem. Rev.*, 1995, **95**, 69–96.
125 J. Yu, Y. Su and B. Cheng, *Adv. Funct. Mater.*, 2007, **17**, 1984–1990.
126 L. Yang, L. Zeng, H. Liu, Y. Deng, Z. Zhou, J. Yu, H. Liu and W. Zhou, *Appl. Catal., B*, 2019, **249**, 98–105.
127 W. Liu, Y. Yang, L. Chen, E. Xu, J. Xu, S. Hong, X. Zhang and M. Wei, *Appl. Catal., B*, 2021, **282**, 119569.
128 J. Wéry, B. Dulieu, E. Launay, J. Bullot, M. Baïtoul and J.-P. Buisson, *Synth. Met.*, 1997, **84**, 277–278.
129 E. J. Horn, B. R. Rosen, Y. Chen, J. Tang, K. Chen, M. D. Eastgate and P. S. Baran, *Nature*, 2016, **533**, 77–81.
130 L. M. Reid, T. Li, Y. Cao and C. P. Berlinguette, *Sustainable Energy Fuels*, 2018, **2**, 1905–1927.
131 L. Zhang, L. Liardet, J. Luo, D. Ren, M. Grätzel and X. Hu, *Nat. Catal.*, 2019, **2**, 366–373.
132 G. Laudadio, Y. Deng, K. van der Wal, D. Ravelli, M. Nuño, M. Fagnoni, D. Guthrie, Y. Sun and T. Noël, *Science*, 2020, **369**, 92–96.
133 Z. Huang, M. Shanmugam, Z. Liu, A. Brookfield, E. L. Bennett, R. Guan, D. E. Vega Herrera, J. A. Lopez-Sanchez, A. G. Slater and E. J. McInnes, *J. Am. Chem. Soc.*, 2022, **144**, 6532–6542.
134 X. Zhao, Z. Li, Y. Chen, L. Shi and Y. Zhu, *Appl. Surf. Sci.*, 2008, **254**, 1825–1829.
135 M. E. Vaschetto, A. P. Monkman and M. Springborg, *J. Mol. Struct.: THEOCHEM*, 1999, **468**, 181–191.
136 D.-W. Sun, K.-L. Chen and J.-H. Huang, *Appl. Catal., A*, 2021, **628**, 118397.
137 M. Han, S. Zhu, C. Xia and B. Yang, *Appl. Catal., B*, 2022, **316**, 121662.
138 V. Rodríguez-González, C. Terashima and A. Fujishima, *J. Photochem. Photobiol., C*, 2019, **40**, 49–67.
139 S. Gelover, P. Mondragón and A. Jiménez, *J. Photochem. Photobiol., A*, 2004, **165**, 241–246.
140 S. Gautam, H. Agrawal, M. Thakur, A. Akbari, H. Sharda, R. Kaur and M. Amini, *J. Environ. Chem. Eng.*, 2020, **8**, 103726.
141 C.-C. Pan and J. C. S. Wu, *Mater. Chem. Phys.*, 2006, **100**, 102–107.
142 G. L. Liu, D. W. Zhu, S. J. Liao, L. Y. Ren, J. Z. Cui and W. B. Zhou, *J. Hazard. Mater.*, 2009, **172**, 1424–1429.
143 R. T. Thomas, V. Nair and N. Sandhyarani, *Colloids Surf., A*, 2013, **422**, 1–9.
144 X. u. Zhao, Z. Li, Y. Chen, L. Shi and Y. Zhu, *J. Mol. Catal. A: Chem.*, 2007, **268**, 101–106.
145 N. P. Gonçalves, M. C. Paganini, P. Armillotta, E. Cerrato and P. Calza, *J. Environ. Chem. Eng.*, 2019, **7**, 103475.
146 W. Wang, P. Serp, P. Kalck and J. L. Faria, *J. Mol. Catal. A: Chem.*, 2005, **235**, 194–199.
147 Y. Ou, J. Lin, S. Fang and D. Liao, *Chem. Phys. Lett.*, 2006, **429**, 199–203.
148 M. M. Kamrannejad, A. Hasanzadeh, N. Nosoudi, L. Mai and A. A. Babaluo, *MATER RES-IBERO-AM J*, 2014, **17**, 1039–1046.
149 M. Inagaki, F. Kojin, B. Tryba and M. Toyoda, *Carbon*, 2005, **43**, 1652–1659.
150 Y.-C. Hsu, H.-C. Lin, C.-W. Lue, Y.-T. Liao and C.-M. Yang, *Appl. Catal., B*, 2009, **89**, 309–314.
151 O. Akhavan, R. Azimirad, S. Safa and M. Larijani, *J. Mater. Chem.*, 2010, **20**, 7386–7392.
152 T. Li, T. Kasahara, J. He, K. E. Dettelbach, G. M. Sammis and C. P. Berlinguette, *Nat. Commun.*, 2017, **8**, 390.
153 J. B. Xia, C. Zhu and C. Chen, *J. Am. Chem. Soc.*, 2013, **135**, 17494–17500.
154 Y. Nakaji, M. Tamura, S. Miyaoka, S. Kumagai, M. Tanji, Y. Nakagawa, T. Yoshioka and K. Tomishige, *Appl. Catal., B*, 2021, **285**, 119805.
155 S. Tian, Y. Jiao, Z. Gao, Y. Xu, L. Fu, H. Fu, W. Zhou, C. Hu, G. Liu, M. Wang and D. Ma, *J. Am. Chem. Soc.*, 2021, **143**, 16358–16363.
156 X. Jie, W. Li, D. Slocombe, Y. Gao, I. Banerjee, S. Gonzalez-Cortes, B. Yao, H. AlMegren, S. Alshihri, J. Dilworth, J. Thomas, T. Xiao and P. Edwards, *Nat. Catal.*, 2020, **3**, 902–912.
157 H. Tong, S. Ouyang, Y. Bi, N. Umezawa, M. Oshikiri and J. Ye, *Adv. Mater.*, 2012, **24**, 229–251.
158 Y. Chen, J. Du and Z. Zuo, *Chem*, 2020, **6**, 266–279.
159 A. Hu, J. J. Guo, H. Pan, H. Tang, Z. Gao and Z. Zuo, *J. Am. Chem. Soc.*, 2018, **140**, 1612–1616.
160 X. J. Wei, I. Abdiaj, C. Sambiagio, C. Li, E. Zysman-Colman, J. Alcazar and T. Noel, *Angew. Chem., Int. Ed. Engl.*, 2019, **58**, 13030–13034.
161 X. Zong, L. Niu, W. Jiang, Y. Yu, L. An, D. Qu, X. Wang and Z. Sun, *Appl. Catal., B*, 2021, **291**, 120099.
162 Z. Mo, J. Di, P. Yan, C. Lv, X. Zhu, D. Liu, Y. Song, C. Liu, Q. Yu, H. Li, Y. Lei, H. Xu and Q. Yan, *Small*, 2020, **16**, e2003914.
163 J. Chen, C. L. Dong, D. Zhao, Y. C. Huang, X. Wang, L. Samad, L. Dang, M. Shearer, S. Shen and L. Guo, *Adv. Mater.*, 2017, **29**, 1606198.
164 X. Fan, L. Zhang, M. Wang, W. Huang, Y. Zhou, M. Li, R. Cheng and J. Shi, *Appl. Catal., B*, 2016, **182**, 68–73.
165 N. Khelidj, X. Colin, L. Audouin, J. Verdu, C. Monchy-Leroy and V. Prunier, *Polym. Degrad. Stab.*, 2006, **91**, 1598–1605.
166 A. François-Heude, E. Richaud, E. Desnoux and X. Colin, *Polym. Degrad. Stab.*, 2014, **100**, 10–20.
167 J. R. White, *C. R. Chim.*, 2006, **9**, 1396–1408.
168 M. Gardette, A. Perthue, J.-L. Gardette, T. Janecska, E. Földes, B. Pukánszky and S. Therias, *Polym. Degrad. Stab.*, 2013, **98**, 2383–2390.

169 T. Dai, Z. Yuan, Y. Meng, B. Xie, Z. Ni and S. Xia, *Appl. Clay Sci.*, 2021, **212**, 106210.
170 B. Ji, G. Yan, W. Zhao, X. Zhao, J. Ni, J. Duan, Z. Chen and Z. Yang, *Ceram. Int.*, 2020, **46**, 20830–20837.
171 W. Diao, H. Cai, L. Wang, X. Rao and Y. Zhang, *ChemCatChem*, 2020, **12**, 5420–5429.
172 Z. Shayegan, F. Haghighat and C.-S. Lee, *J. Environ. Chem. Eng.*, 2020, **8**, 104162.
173 J. Zhang, K. Vikrant, K.-H. Kim, F. Dong, M. W. Chung and S. Weon, *Chem. Eng. J.*, 2022, **439**, 135747.